Predecessor Rain Events ahead of Tropical Cyclones

THOMAS J. GALARNEAU JR. AND LANCE F. BOSART

Department of Atmospheric and Environmental Sciences, University at Albany, State University of New York, Albany, New York

RUSS S. SCHUMACHER

Department of Atmospheric Sciences, Texas A&M University, College Station, Texas

(Manuscript received 6 October 2009, in final form 8 March 2010)

ABSTRACT

Twenty-eight predecessor rain events (PREs) that occurred over the United States east of the Rockies during 1995–2008 are examined from a synoptic climatology and case study perspective. PREs are coherent mesoscale regions of heavy rainfall, with rainfall rates $\geq$100 mm (24 h)$^{-1}$, that can occur approximately 1000 km poleward of recurving tropical cyclones (TCs). PREs occur most commonly in August and September, and approximately 36 h prior to the arrival of the main rain shield associated with the TC. A distinguishing feature of PREs is that they are sustained by deep tropical moisture that is transported poleward directly from the TC. PREs are high-impact weather events that can often result in significant inland flooding, either from the PRE itself or from the subsequent arrival of the main rain shield associated with the TC that falls onto soils already saturated by the PRE.

The composite analysis shows that on the synoptic-scale, PREs form in the equatorward jet-entrance region of a 200-hPa jet on the western flank of a 925-hPa equivalent potential temperature ridge located east of a 700-hPa trough. On the mesoscale, PREs occur in conjunction with low-level frontogenetical forcing along a baroclinic zone where heavy rainfall is focused. A case study analysis was conducted of a PRE ahead of TC Erin (2007) that produced record-breaking rainfall (>250 mm) from southern Minnesota to Lake Michigan. This analysis highlighted the importance of frontogenetical forcing along a low-level baroclinic zone in the presence of deep tropical moisture from TC Erin in producing a long-lived, quasi-stationary mesoscale convective system.

1. Introduction

a. Motivation and PRE overview

Cote (2007) first defined the term predecessor rain event (PRE) to describe meso- and subsynoptic-scale regions of high-impact heavy rainfall that occur well in advance of recurving tropical cyclones (TCs) over the eastern third of the United States. PREs pose a difficult forecasting challenge because operational models can have difficulty properly representing mesoscale regions of heavy rainfall in space and time, and the mesoscale features that serve to focus the heavy precipitation can often be underanalyzed or missed altogether. The high-impact nature of PREs was underscored by the PRE that occurred over New York City on the morning of 8 September 2004 in advance of TC Frances (Fig. 1a). This high-impact PRE was the subject of a front-page article in the *New York Times* the following day (Luo 2004), highlighting the large societal impact PREs can pose in addition to the inherent forecasting challenge (Fig. 1b).

Cote (2007) examined all recurving TCs over the eastern third of the United States and extreme western North Atlantic (defined as the Atlantic, Caribbean, and Gulf of Mexico basins) during 1998–2006, and manually selected cases in which a PRE occurred. He defined a PRE as a coherent region of heavy rainfall, with rainfall rates exceeding 100 mm in 24 h that was positioned poleward and was separate from the main rain shield associated with the TC. An important aspect of a PRE is that deep tropical moisture, typically manifested as total column precipitable water (PW) values greater than 50 mm, originally associated with the TC must be advected poleward

Corresponding author address: Thomas J. Galarneau Jr., Department of Atmospheric and Environmental Sciences, University at Albany, State University of New York, ES-351, 1400 Washington Ave., Albany, NY 12222.
E-mail: tomjr@atmos.albany.edu

DOI: 10.1175/2010MWR3243.1

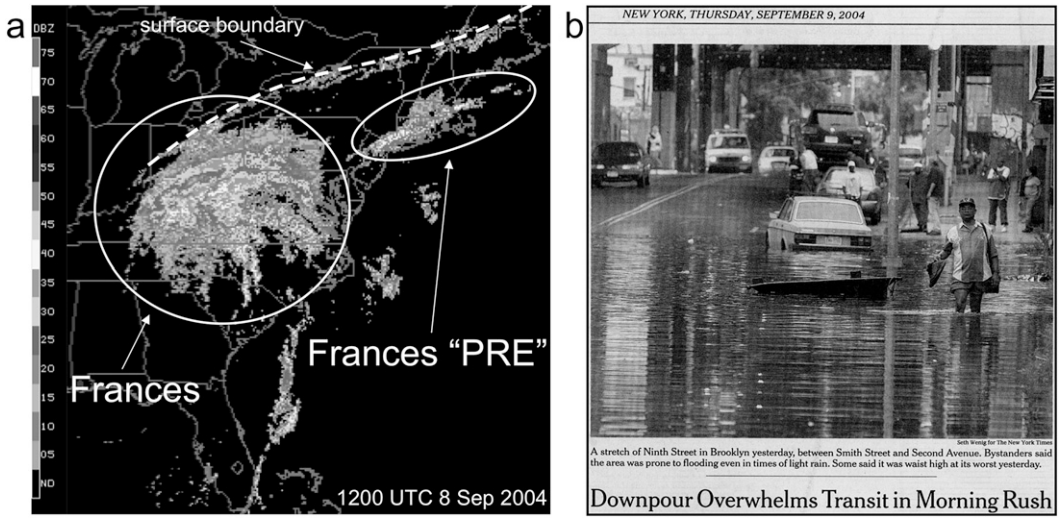

FIG. 1. (a) WSI NOWrad base reflectivity mosaic (shaded according to the grayscale in dB*Z*) at 1200 UTC 8 Sep 2004. TC Frances, the Frances PRE, and a surface boundary are labeled. (b) Front page photo and article highlighting the flooding from the high-impact TC Frances PRE (©2004, *The New York Times*).

into the PRE region. Cote (2007) documented 47 PREs that occurred in association with 21 TCs; overall one-third of all recurving TCs were associated with at least one PRE.

Of the 47 documented PREs in Cote (2007), 26 occurred left of the TC track (LOT), while 12 were along track (AT) and 9 were right of track (ROT). The track-relative position takes into account the entire TC track, rather than just the TC track up to the time of PRE initiation. These PREs were located on average 1000 km poleward of the TC at the time of PRE initiation, and occurred approximately 36 h prior to the arrival of the TC at the latitude of the PRE. Geography-relative composite analyses of PREs associated with recurving TCs over the eastern United States and western North Atlantic by Cote (2007) showed that 1) PREs were associated with the poleward transport of deep tropical moisture ahead of the recurving TC, and 2) PREs occurred where this deep tropical moisture intersected a region of forced ascent over and north of a low-level baroclinic zone situated beneath an equatorward jet-entrance region.

The composite synoptic-scale flow pattern presented in Cote (2007) agrees quite well with the upper-level flow pattern schematic presented in a study of antecedent rainfall associated with TC Agnes (1972) by Bosart and Carr (1978, see their Fig. 2). The TC Agnes rain event was likely the first detailed analysis of a PRE, although a major rain event was documented to have occurred over Massachusetts, Connecticut, and Rhode Island during 17–21 September 1938 ahead of the historic New England TC (Pierce 1939). Antecedent rainfall ahead of TC Marco (1990) east of the Appalachians over North and South Carolina was likely a PRE as well (Srock and Bosart 2009), and highlights the importance of terrain features, mesoscale surface boundaries, and coastal fronts as possible focusing mechanisms for some PREs. The occurrence of PREs is not limited to TCs originating over the North Atlantic. Western North Pacific TC Songda (2004) contributed deep tropical moisture to a PRE over Japan (Wang et al. 2009), while the frequent contribution of deep tropical moisture from eastern North Pacific TCs to southwestern U.S. rainfall events (Corbosiero et al. 2009) likely sets the stage for occasional PREs.

The purpose of this paper is to examine the typical synoptic and mesoscale environments associated with PREs through a synoptic climatology and case study analysis. Cote's (2007) case list will be expanded to include all PREs that occurred over the central and eastern United States in association with recurving North Atlantic TCs during 1995–2008. This expanded case list will be used to construct PRE-relative composites to better identify characteristic environmental flow structures associated with PREs.

A detailed case study of the high-impact PRE associated with TC Erin (2007) will also be presented to build upon the results of the composite analysis and highlight additional physical processes governing PRE evolution.

b. Previous research on heavy rainfall

The synoptic and mesoscale conditions in which high-impact heavy rain events occur are well documented (e.g., Maddox et al. 1979; Doswell et al. 1996; Brooks and Stensrud 2000; Schumacher and Johnson 2005, 2006). Heavy rain events often occur beneath the equatorward

TABLE 1. Details of all documented PREs over the United States east of the Rockies associated with North Atlantic TCs during 1995–2008. The PRE parent TC, year, initiation date and time (UTC), location relative to the parent TC track, jet structure, and geographical location are listed. Left of TC track (LOT), along TC track (AT), right of TC track (ROT), anticyclonically curved (AC) 200-hPa jet (boldface), cyclonically curved (CC) 200-hPa jet (normal text), and unclassifiable jet structure (N/A, italics).

TC (Yr)	Initiation (UTC)	Location relative to track	Jet structure	Geographic location
Opal (1995)	**0000 UTC 3 Oct**	**LOT**	**AC**	**TX/LA/MS**
Fran (1996)	*0600 UTC 4 Sep*	*AT*	*N/A*	*NC*
Danny (1997)	0000 UTC 23 Jul	AT	CC	NC
Bonnie (1998)	0600 UTC 26 Aug	LOT	CC	NY/PA
Bret (1999)	1800 UTC 23 Aug	ROT	CC	TX
Floyd (1999)	1800 UTC 14 Sep	LOT	CC	SC/NC/VA
Harvey (1999)	*1800 UTC 20 Sep*	*LOT*	*N/A*	*GA/SC*
Helene (2000)	1800 UTC 20 Sep	ROT	CC	GA
Lili (2002)	**1200 UTC 2 Oct**	**LOT**	**AC**	**OK/KS/NE/IA**
Grace (2003)	**0000 UTC 31 Aug**	**LOT**	**AC**	**OK/KS/MO**
Isabel (2003)	1800 UTC 16 Aug	ROT	CC	NY/MA/CT/RI/VT/NH
Alex (2004)	*1800 UTC 2 Aug*	*LOT*	*N/A*	*NC/VA*
Bonnie (2004)	**1200 UTC 12 Aug**	**AT**	**AC**	**GA/SC/NC/VA/PA/NY**
Charley (2004)	1200 UTC 13 Aug	LOT	CC	FL/GA/SC
Frances (2004)	**0600 UTC 8 Sep**	**ROT**	**AC**	**NY**
Gaston (2004)	**1800 UTC 30 Aug**	**LOT**	**AC**	**NY**
Jeanne (2004)	**0600 UTC 28 Sep**	**LOT**	**AC**	**PA/NY/MA/CT/RI**
Matthew (2004)	**1800 UTC 7 Oct**	**AT**	**AC**	**AR/MO/LA**
Dennis (2005)	1800 UTC 9 Jul	AT	CC	FL/GA/SC
Irene (2005)	**0000 UTC 15 Aug**	**LOT**	**AC**	**NY/CT/RI**
Katrina (2005)	**0600 UTC 29 Aug**	**AT**	**AC**	**KY**
Ophelia (2005)	**1200 UTC 15 Sep**	**LOT**	**AC**	**NY/RI/MA**
Rita (2005)	**0000 UTC 25 Sep**	**LOT**	**AC**	**NE/SD/IA/MN/WI**
Wilma (2005)	**0000 UTC 24 Oct**	**LOT**	**AC**	**GA/SC**
Alberto (2006)	**1800 UTC 12 Jun**	**AT**	**AC**	**NC/SC**
Ernesto (2006)	**1800 UTC 30 Aug**	**LOT**	**AC**	**NC**
Erin (2007)	**0000 UTC 19 Aug**	**LOT**	**AC**	**MN/WI/IL**
Ike (2008)	**0600 UTC 13 Sep**	**LOT**	**AC**	**MO/IL/IN/OH**

jet-entrance region of an upper-level jet streak where broad quasigeostrophic (QG) forcing for ascent can provide a favorable environment for deep-layer moistening and destabilization (e.g., Uccellini and Johnson 1979; Bosart and Lackmann 1995). Within this favorable synoptic-scale environment, mesoscale features such as baroclinic zones (e.g., Maddox et al. 1979; Glass et al. 1995; Junker et al. 1999; Moore et al. 2003; Schumacher and Johnson 2005, 2006) and mountain barriers (e.g., Maddox et al. 1978; Caracena et al. 1979; Pontrelli et al. 1999) can act as focusing mechanisms for vigorous ascent. In both circumstances, a low-level jet is important in advecting warm, moist air in to the region of heavy precipitation. Furthermore, a low-level jet oriented perpendicular to a surface boundary can result in enhanced low-level warm advection and moisture convergence and associated vigorous ascent (e.g., Maddox et al. 1979; Augustine and Caracena 1994; Trier et al. 2006).

Slow-moving mesoscale convective systems (MCSs; Maddox 1980) that occur on the cool side of zonally oriented surface baroclinic zones can produce particularly extreme rainfall and cause devastating flash floods (e.g., Chappell 1986; Doswell et al. 1996). In this scenario, deep moist convection can repeatedly move over a given area, commonly termed as ''training echoes'' (e.g., Davis 2001). Schumacher and Johnson (2005) classified these types of MCSs as ''trailing line/adjoining stratiform,'' where a convective line develops that is oriented parallel to the upper-level wind shear vector and new convective cells repeatedly form on the upshear side of the MCS and subsequently move downshear.

Heavy rainfall and flooding can also occur directly from the passage of a TC, or from the interaction of the TC vortex with a baroclinic zone or mountain barrier. Examples of such extreme rain events include TCs Connie (1955; Dunn et al. 1955), Diane (1955; Namias and Dunn 1955; Chapman and Sloan 1955), Camille (1969; Schwarz 1970), Agnes (1972; Bosart and Carr 1978; Carr and Bosart 1978; Bosart and Dean 1991), Alberto (1994; Avila and Rappaport 1996), Floyd (1999; Atallah and Bosart 2003; Colle 2003), Allison (2001; Beven et al. 2003), and Alberto (2006; Franklin and Brown 2008). The heavy rainfall produced from these TCs occurred in a wide range of conditions, for example, a ridge environment

with weak flow resulting in a nearly stationary system as with TC Alberto (1994), or heavy precipitation forming as a result of extratropical transition (ET) as in TC Floyd (1999). The former condition can behave very much like the flash-flood-producing mesoscale convective vortices described by Schumacher and Johnson (2008, 2009). The latter condition occurs in response to warm air advection and upward-increasing cyclonic vorticity advection in the presence of deep tropical moisture as the TC undergoes ET (e.g., Jones et al. 2003 and references within; Atallah et al. 2007). The distinguishing factor between these TC-related heavy rain events and PREs is that PREs are displaced well poleward of TCs, outside of the direct influence of the TCs cyclonic circulation.

c. *Outline of paper*

The remainder of this paper is organized as follows. The datasets and methods used to construct the composite analyses along with the diagnostic analysis procedures employed are described in section 2. Section 3 presents the statistics and composite analyses for all PREs that occurred over the United States east of the Rockies during 1995–2008. Section 4 presents a multiscale case analysis of a PRE associated with TC Erin on 19 August 2007. Finally, section 5 summarizes the key findings presented in the paper and provides concluding remarks.

2. Data and methods

a. *Case identification and stratification*

The analysis shown here is expanded from Cote (2007) to include all PREs from 1995 to 2008 over the United States east of the Rockies and focuses only on the initial PRE for each parent TC (Table 1). The focus on the initial PRE was done in order to mitigate the bulk upscale effect of deep moist convection associated with the PRE itself on the composite fields, and to assure that each PRE parent TC in the dataset carried equal weight in the composite since some TCs produced multiple PREs while others did not. Coherent areas of rainfall were selected as PREs based on the following criteria as in Cote (2007):

- Radar reflectivity values ≥35 dBZ within a coherent area of rainfall persisting for at least 6 h.
- The average rainfall must be ≥100 mm $(24\ \text{h})^{-1}$ over the entire life of the PRE.
- While there is no objective TC–PRE separation distance required, the following two criteria must be met:
  - There must be a clear separation on the radar imagery between the coherent area of rainfall and the TC rain shield.
  - Deep tropical moisture directly associated with the TC must be advected away from the TC into the region of the coherent area of rainfall.

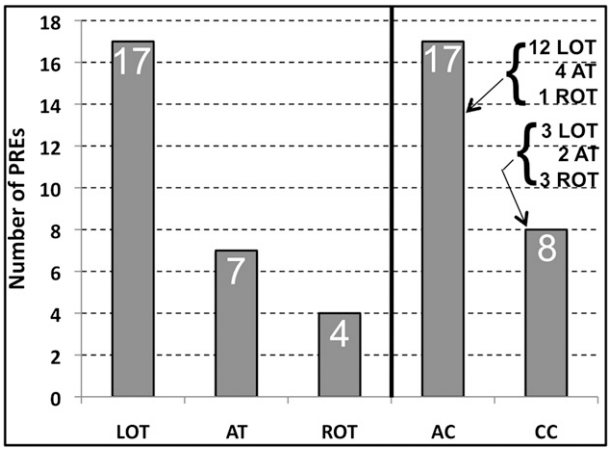

FIG. 2. Histogram of the 28 PREs that occurred during 1995–2008 (listed in Table 1), stratified by their location relative to the TC track [left of track (LOT); along track (AT); and right of track (ROT)] and the structure of the 200-hPa jet [anticyclonically curved jet (AC); cyclonically curved jet (CC)]. The jet structure for 3 of the PREs was unclassifiable.

Radar characteristics were determined by manually examining the national base reflectivity mosaic imagery available at the National Climatic Data Center (NCDC) and the National Center for Atmospheric Research (NCAR) case selection archive. Rainfall amounts were determined by using the quantitative precipitation estimate (QPE) data available from the National Oceanic and Atmospheric Administration (NOAA) National Precipitation Verification Unit (NPVU) for cases 2001 and later, and the NCEP unified precipitation dataset (UPD; Higgins et al. 2000) for cases prior to 2001.

To assess whether the deep tropical moisture originated directly from the TC, PW analyses were generated using the (National Centers for Environmental Prediction) NCEP–NCAR reanalysis dataset (Kalnay et al. 1996; Kistler et al. 2001) at 2.5° × 2.5° horizontal resolution. Observed atmospheric soundings archived at the University of Wyoming and twice-daily synoptic charts archived at the Storm Prediction Center and at the University at Albany were also used to help verify the model analyses.

The PREs that were selected based upon the above criteria were then stratified by the location of the PRE relative to the TC track and by the curvature of the 200-hPa jet over and near the PRE region at the closest 6-h analysis time to PRE initiation (Table 1). The former type of categorization—LOT, AT, and ROT—was used to link back to previous studies that made reference to the location of heavy precipitation directly associated

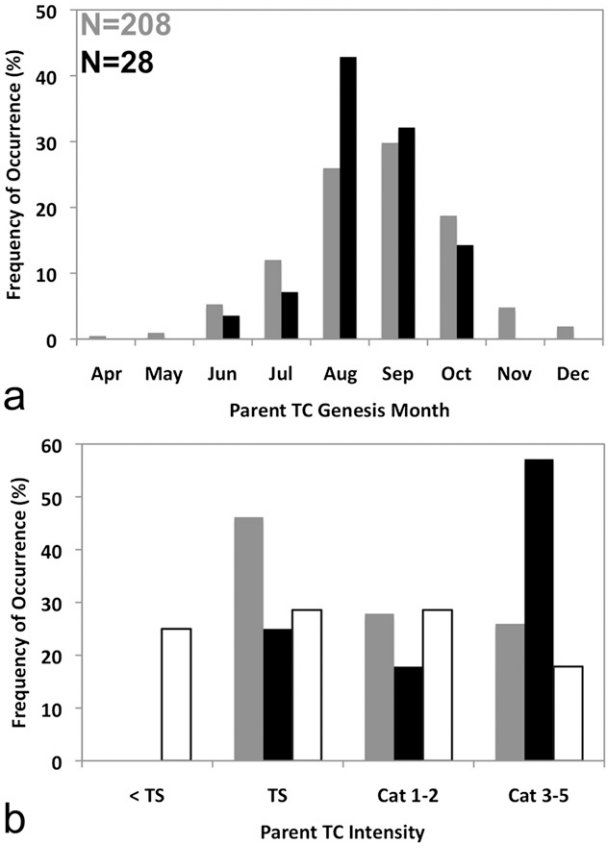

FIG. 3. (a) Histogram of the monthly frequency distribution of all TCs (gray bars) and TCs that produced PREs (black bars) during 1995–2008. (b) As in (a), but shows maximum TC intensity Saffir–Simpson scale category. Additionally, (b) shows the TC intensity at the time of PRE initiation (clear bars).

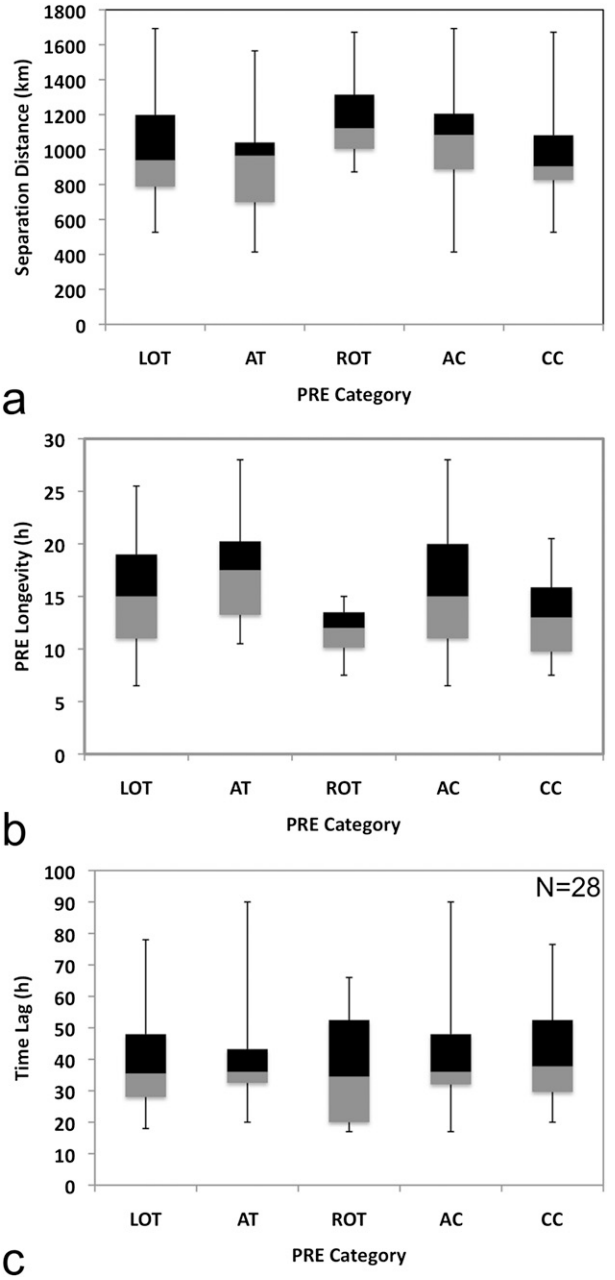

FIG. 4. Box and whisker diagrams of (a) TC–PRE separation distance (km), (b) PRE longevity (h), and (c) time lag between PRE occurrence and TC passage (h), for all PREs stratified by the categories shown on Fig. 2. The lower (upper) bound of the box marks the 25th (75th) percentile, and the transition from black to gray in the box marks the median value. The whiskers mark the maximum and minimum values.

with TCs (e.g., Atallah et al. 2007). The TC track-relative stratification also helps indicate how often TC rainfall passes directly over the same region previously affected by the PRE. Of the 28 documented PREs during 1995–2008, 17 occurred LOT while 7 and 4 occurred AT and ROT, respectively (Fig. 2). The AT PREs can be particularly devastating to life and property since high-impact flooding is more likely to occur in response to TC rain passing over regions where the soil was previously saturated by the PRE.

Upper-level jets were categorized as anticyclonically curved (AC) or cyclonically curved (CC) at 200 hPa to stratify the PREs with a similar synoptic-scale flow pattern configuration. The AC category was typically associated with a well-defined upper-level ridge and a strong anticyclonically curved jet maximum east of the PRE, and an upper-level trough west of the PRE. The CC category was typically associated with a much larger-scale upper-level trough relative to the AC category west of the PRE with an attendant cyclonically curved upper-level jet maximum. The CC PREs typically moved faster and were associated with more widespread stratiform precipitation (e.g., TC Floyd 1999) compared to AC PREs, which were more frequently associated with slower-moving backbuilding convective systems (e.g., TC Erin

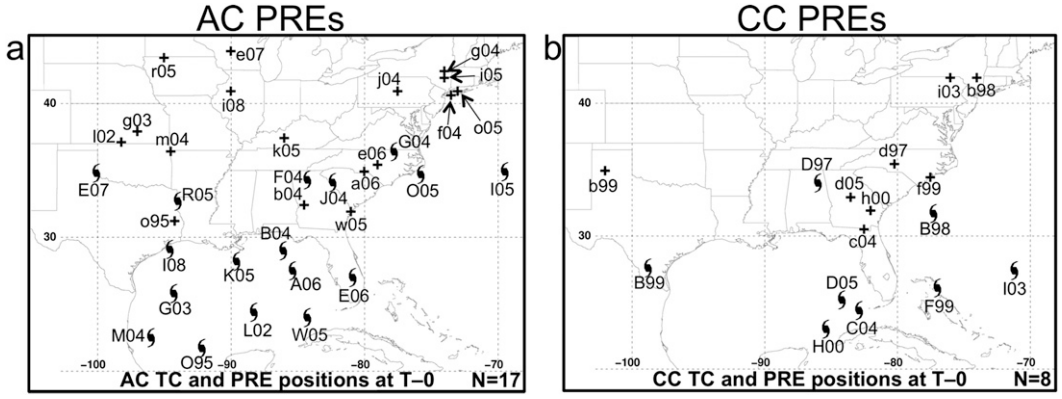

FIG. 5. Geographical locations of all PRE parent TCs and their initial PREs (any subsequent PREs were not considered) during 1995–2008 at the time of PRE initiation for (a) AC and (b) CC PREs. PREs (lowercase; + symbols) and TCs (uppercase; TC symbols) are labeled by the first letter of the parent TC and the two-digit year.

2007). Figure 2 also shows the frequency of AC and CC PREs; 17 and 8 PREs were associated with anticyclonically and cyclonically, respectively, curved jets (3 PREs were unclassifiable). PREs in the AC category (i.e., 17) occur preferentially LOT (12 out of 17), while PREs in the CC category (i.e., 8) are more evenly distributed relative to the TC track (Fig. 2).

b. Composite analysis

The composite analyses were generated using the 6-hourly NCEP–NCAR reanalysis dataset at the analysis time closest to PRE initiation ($T - 0$), 24 h prior to PRE initiation ($T - 24$), and 24 h after PRE initiation ($T + 24$). Composites were also generated for 12 h prior to PRE initiation ($T - 12$) to examine upper-level jet intensification leading up to $T - 0$. The grids for each case were shifted prior to compositing so that the centroid of the PRE initiation location, determined by radar imagery, was located at the median location for all AC PREs (38°N, 85°W). The composite analysis presented in section 3b will only describe the results from the AC PRE category since the CC category has relatively few (i.e., 8) members and the broad upstream trough seemingly characteristic of CC PREs failed to show statistical significance (likely due to the varying amplitude and relative location of the trough among the CC PRE cases).

To assess the role of QG forcing for ascent in the PRE environment in the composite, the right-hand side of the **Q** vector form of the QG omega equation (Hoskins et al. 1978) was evaluated at 700 hPa, less the Beta term [Bluestein 1992, see his Eq. (5.7.56)]:

$$-\frac{1}{2}\left(\nabla_p^2 + \frac{f_0^2}{\sigma}\frac{\partial^2}{\partial p^2}\right)\omega = \nabla_p \cdot \mathbf{Q}, \tag{1}$$

where **Q** is defined as [Bluestein 1992, see his Eq. (5.7.55)]:

$$\mathbf{Q} = -\frac{R}{\sigma p}\begin{pmatrix} \dfrac{\partial \mathbf{V}_g}{\partial x}\cdot\nabla_p T \\ \dfrac{\partial \mathbf{V}_g}{\partial y}\cdot\nabla_p T \end{pmatrix} = \begin{pmatrix} Q_1 \\ Q_2 \end{pmatrix}. \tag{2}$$

The variables in these equations have their usual meteorological meanings. Regions of $\nabla_p \cdot \mathbf{Q} < 0$ (>0) from (1) are indicative of QG forcing for ascent (descent) at 700 hPa.

Additionally, the Petterssen frontogenesis equation for the rate of change of the magnitude of the horizontal potential temperature θ gradient in horizontal, adiabatic flow was computed to assess the role of frontogenesis in focusing vertical motion and associated precipitation in the PRE. Following the notation by Keyser et al. (1986, p. 840), the Petterssen frontogenesis equation can be written as

$$\frac{d}{dt_h}|\nabla_h\theta| = -\frac{1}{2}|\nabla_h\theta|(D_h - F_h\cos 2\beta_h), \tag{3}$$

where the subscript h represents the horizontal plane and the quantities D_h and F_h denote the divergence and the magnitude of the resultant deformation, respectively. The angle β_h is defined as the difference between the angles of the local orientation of the axis of dilatation and the isentropes in the horizontal plane. The deformation term can contribute to frontogenesis when $|\beta_h| < 45°$.

c. Case study

The TC Erin (2007) PRE was chosen for further study because it represents typical synoptic and mesoscale forcing mechanisms apparent in AC PREs; in particular AC PREs that produce backbuilding slow-moving convective systems. This case study required the synthesis of several observational datasets, including: (i) National

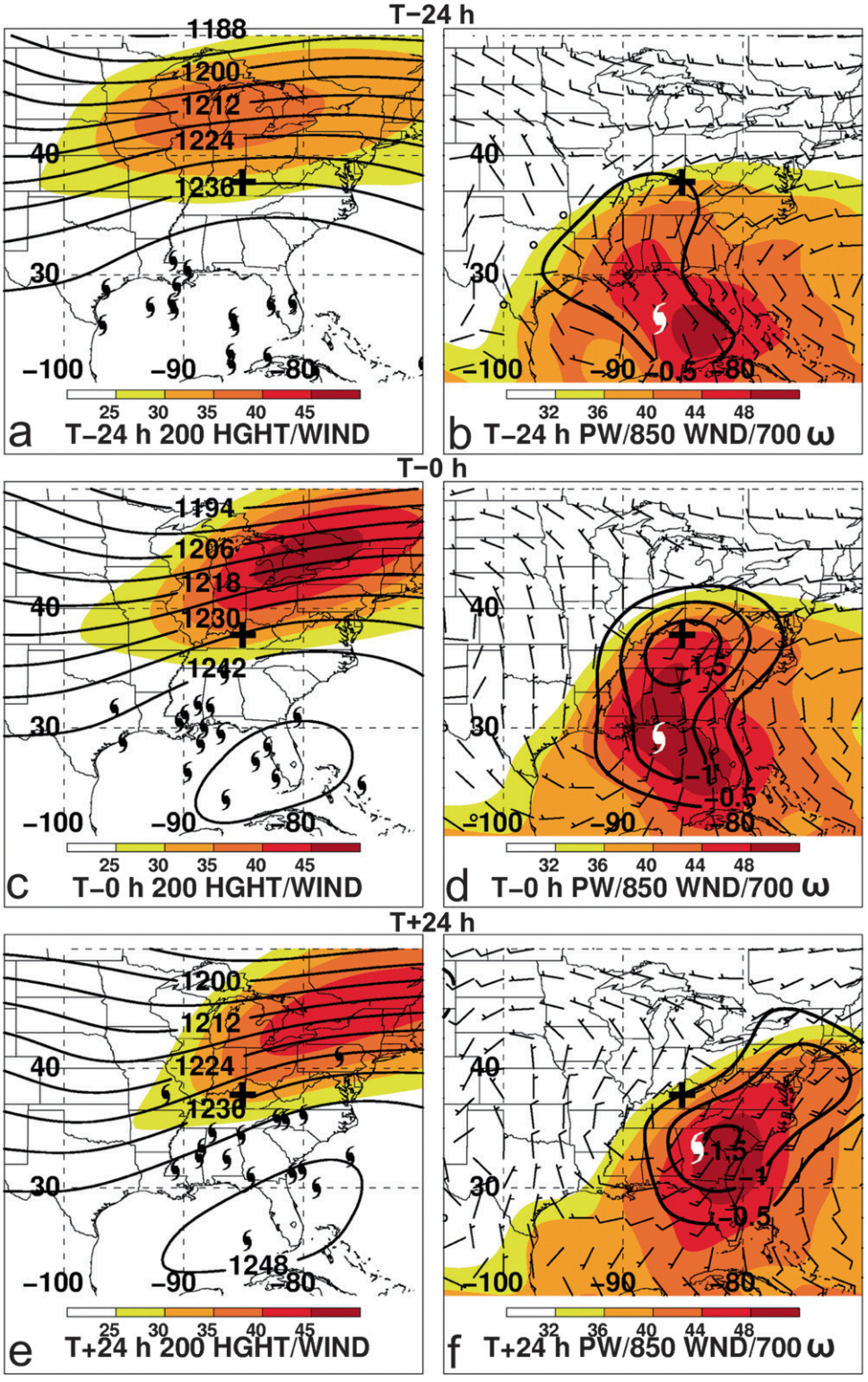

FIG. 6. PRE-relative composite for the 17 AC PREs during 1995–2008 of 200-hPa geopotential height (solid contours every 6 dam) and wind speed (shaded according to the color bar in m s^{-1}) at (a) $T - 24$, (c) $T - 0$, and (e) $T + 24$, and total column PW (shaded in mm), 700-hPa vertical motion (upward motion in black contours every 0.5×10^{-3} hPa s^{-1} starting at -0.5×10^{-3} hPa s^{-1}), and 850-hPa wind (half barb = 2.5 m s^{-1}; full barb = 5.0 m s^{-1}; pennant = 25.0 m s^{-1}) at (b) $T - 24$, (d) $T - 0$, and (f) $T + 24$. The composite PRE initiation location is marked with a black + symbol, the parent TC PRE-relative locations are labeled with black TC symbols, and the median parent TC PRE-relative locations are labeled with white TC symbols.

Hurricane Center best-track data (Jarvinen et al. 1984), (ii) standard hourly Automated Surface Observing System (ASOS) observations and twice-daily radiosonde data (archived at the University at Albany), (iii) 6-h temporal and 4-km horizontal resolution gridded QPE data (archived at NPVU), (iv) Weather Surveillance Radar-1988 Doppler (WSR-88D) level-III data (archived at NCDC), (v) *Geostationary Operational Environmental Satellite-12 (GOES-12)* infrared imagery (available from NCAR case selection archive), and (vi) Global Positioning System-Meteorology Observing Systems (GPS-Met) PW data (available from the NOAA/Global Systems Division).

Synoptic analyses and diagnostic calculations were generated using the NCEP Global Forecast System (GFS) analyses available at 6-h intervals and at 0.5° × 0.5° horizontal and 50-hPa (25 hPa in lowest 100 hPa) vertical resolution. Additionally, the NCEP GFS was used for analysis of the transport of deep tropical moisture after being verified by the satellite-derived NOAA/National Environmental Satellite, Data and Information Service (NESDIS) Blended Total PW (TPW) product (available online at http://www.osdpd.noaa.gov/bTPW/). To further assess the transport of deep tropical moisture, the NCEP GFS analysis was also used at 6-hourly intervals to compute backward air parcel trajectories, with linear temporal interpolation used at 2-hourly time steps between analysis periods. The Rapid Update Cycle (RUC) analyses, available at 1-h intervals and at 20-km horizontal and 25-hPa vertical resolution, were used to calculate the 0–6-km wind shear at 3-h intervals. As in the composite analysis, QG forcing for ascent was computed via the right-hand side of the QG omega equation.

3. Synoptic climatology of PREs during 1995–2008

a. PRE statistics

Twenty-eight PREs were documented over the United States east of the Rockies during 1995–2008. Approximately 30% of all TCs that passed west of 70°W and north of 20°N in the North Atlantic during 1995–2008 produced at least one PRE. PREs occurred preferentially with TCs that formed in August and September, with 43% and 32% of all PREs occupying those months, respectively (Fig. 3a), compared with 32% and 30% of all TCs. Nearly 57% of PREs were associated with strong TCs that reach at least category 3 intensity, while 25% and 18% occur with TCs that reach tropical storm (TS) and category 1–2 intensity, respectively (Fig. 3b). The distribution for TC intensity at the time of PRE initiation suggests a general weakening of most TCs from the maximum TC intensity, with 25% of all PRE parent TCs

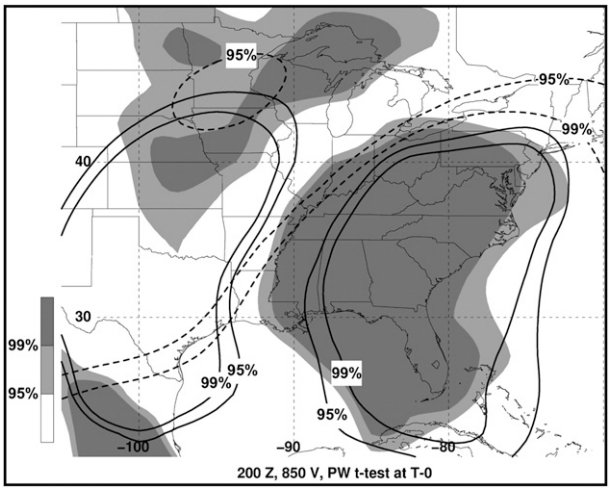

FIG. 7. Statistical significance, which gives the probability that the composite is statistically different from the weighted monthly long-term (1948–2008) climatology at $T - 0$, of PW (shaded according to the grayscale), 850-hPa meridional wind component (solid contours at 95% and 99%), and 200-hPa geopotential height (dashed contours at 95% and 99%).

weaker than TS strength at the time of PRE initiation. Also noteworthy is the apparent weakening of the strong category 3–5 TCs by the time of PRE initiation (Fig. 3b). This weakening of PRE parent TCs may be due to increased deep-layer wind shear associated with the approaching upper-level trough, or due to landfall of the PRE parent TC (8 of the 15 parent TCs in the TS and <TS intensity categories had made landfall prior to PRE initiation).

The TC–PRE separation distance, PRE longevity, and time lag between PRE occurrence and arrival of the parent TC at the latitude of the PRE is shown in Fig. 4, stratified by the categories shown in Fig. 2. The median separation distance between the PRE and parent TC is approximately 1000 km for PREs in all categories, with the shortest (longest) separation distance of 410 km (1700 km) in the AT and AC (LOT and AC) categories (Fig. 4a). The median PRE longevity ranged from 12 to 17.5 h among the PRE categories, with the shortest-lived (longest lived) PRE lasting 6.5 h (28 h) in the AT and AC (LOT and AC) categories (Fig. 4b). The median time lag between PRE occurrence and the passage of the parent TC over or near the PRE region (some TCs did not pass directly over the PRE region) was approximately 36 h for all PRE categories, with the shortest (longest) time lag of 17 h (90 h) in the ROT and AC (AT and AC) categories (Fig. 4c).

b. PRE composite analysis

Figure 5 shows the geographical distribution of AC and CC PREs and their parent TCs at the time of PRE

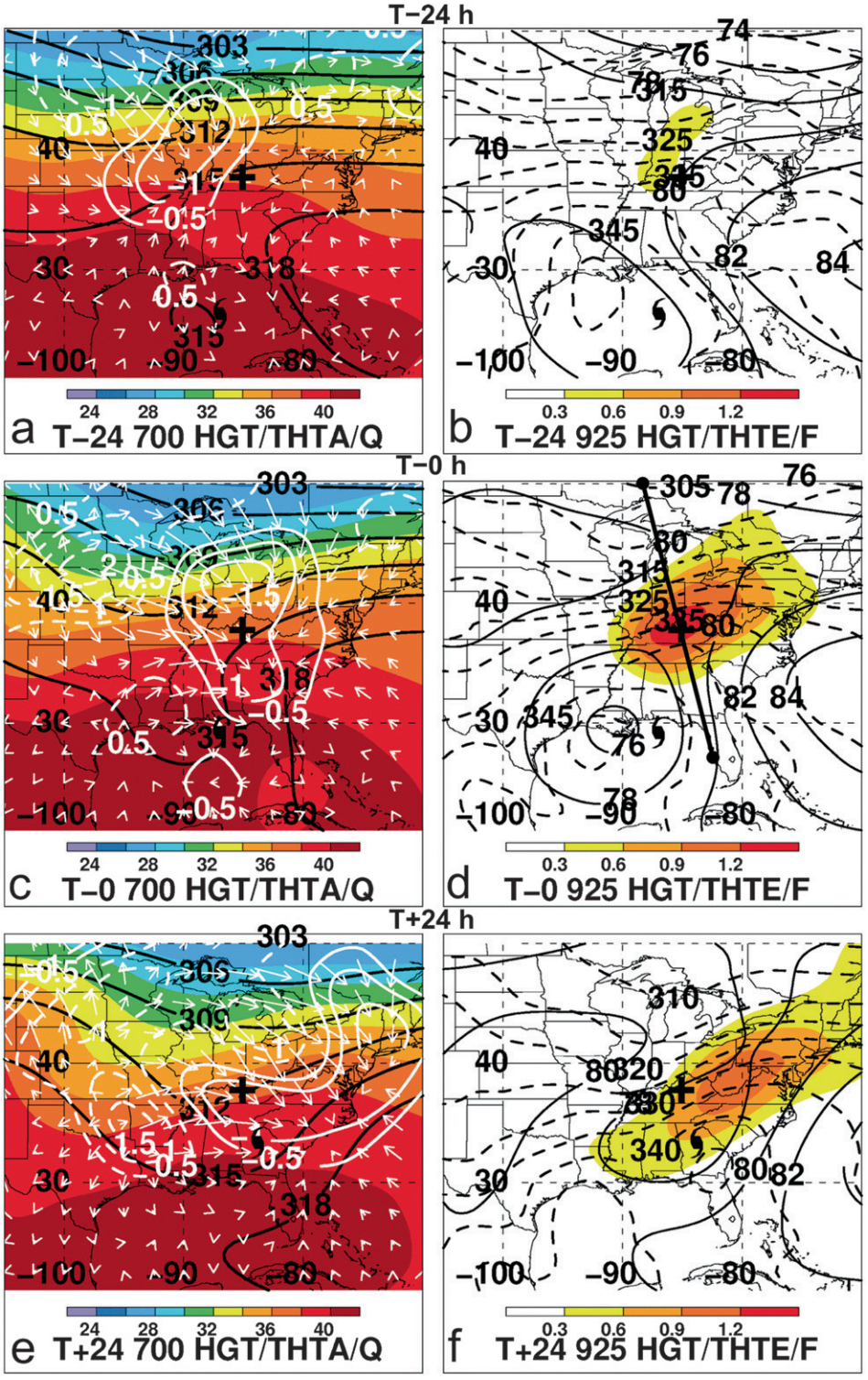

FIG. 8. As in Fig. 6, but for 700-hPa geopotential height (solid contours every 3 dam), potential temperature (shaded according to the color bar in °C), **Q** vectors (arrows in 10^{-8} Pa m^{-1} s^{-1}), and $\nabla\cdot\mathbf{Q}$ (white contours every 0.5×10^{-12} Pa m^{-2} s^{-1}; dashed > 0, solid < 0) at (a) $T - 24$, (c) $T - 0$, and (e) $T + 24$, and 925-hPa geopotential height (solid contours every 2 dam), equivalent potential temperature (dashed contours every 5 K), and Petterssen frontogenesis [shaded according to the color bar in 10^{-1} K (100 km)$^{-1}$ (3 h)$^{-1}$] at (b) $T - 24$, (d) $T - 0$, and (f) $T + 24$. The composite PRE initiation location is marked with a black + symbol and the median parent TC PRE-relative locations are labeled with black TC symbols. The cross section orientation for Fig. 9 is labeled in (d).

initiation. The AC PREs occur throughout the eastern two-thirds of the continental United States, with 13 of 17 PRE parent TCs making landfall along the Gulf of Mexico coastline. Of the 13 TCs that made landfall along the Gulf of Mexico coastline, 8 produced PREs west of the Appalachians. In contrast, CC PREs occur preferentially east of the Appalachians in association with TCs that recurve in the extreme eastern Gulf of Mexico and western Atlantic, with the exception of TC Bret (1999). To assess the typical synoptic- and subsynoptic-scale flow patterns and physical forcing mechanisms associated with PREs, composites were generated in coordinates relative to the PRE initiation location for the 17 AC PREs (Fig. 5a and Table 1) that occurred during 1995–2008. To illustrate the time evolution of the composite fields, the composites were computed at $T - 24$, $T - 0$, and $T + 24$ h in relation to the PRE initiation time.

1) Flow field and moisture structure

Figure 6 shows the structure and evolution of the composite 200-hPa jet structure and tropical PW plume. The composite PRE initiates within the equatorward jet entrance region on the anticyclonic shear side of an intensifying 200-hPa jet that reaches 45 m s^{-1} by $T - 0$ (Figs. 6a,c). The PRE is positioned east of a broad 200-hPa trough, and northwest of a 200-hPa ridge. A two-sided Student's t test, which gives the probability that the composite is statistically different from the weighted monthly long-term (1948–2008) climatology, indicated that the 200-hPa ridge east of the PRE was statistically significant at the 99% level (Fig. 7). Although the PRE-relative positions of the parent TCs have a relatively large zonal variability, many of the TCs cluster approximately 1000 km south-southwest of the PRE and recurve northwestward by $T + 24$ (Figs. 6a,c,e). At $T - 0$, the median AC PRE separation distance was 1080 km, while the median AC PRE longevity was 15 h and the median time lag between the AC PRE and passage of the parent TC was 36 h (Fig. 4).

The composite PW analysis indicates that deep tropical moisture (>44 mm) in which the TC is embedded at $T - 24$, is advected poleward from the TC to the PRE region by the 850-hPa southerly 10 m s^{-1} flow by $T - 0$ (Figs. 6b,d). A Student's t test indicated that the southerly meridional flow at 850 hPa and the PW values south and east of the PRE were statistically significant to the 99% level (Fig. 7). The veering of the wind from southerly at 850 hPa to west-southwesterly at 200 hPa also suggests that warm-air advection is likely an important physical mechanism in driving the ascent in the PRE region (Figs. 6c,d). By $T + 24$, the deep tropical moisture and ascent move east of the PRE initiation location in response to veering of the 850-hPa flow to southwesterly (Figs. 6e,f). The composite also indicates that the 200-hPa jet northeast of the PRE initiation location weakens to 40 m s^{-1} between $T - 0$ and $T + 24$ (Figs. 6c,e). Examination of individual cases reveals that this jet weakening may be an artifact of the composite since 9 out of 17 AC PREs have stronger upper-level jets at $T + 24$ versus $T - 0$, while 4 jets weaken and 4 remain unchanged (not shown). The weakening of the jet in the composite occurred because the jet in many of the individual cases moved well downstream outside of the composite domain by $T + 24$. The weakening or eastward displacement of the upper-level jet maximum (and the attendant synoptic-scale forcing) relative to the composite PRE location by $T + 24$ is likely an important factor in the dissipation of PREs.

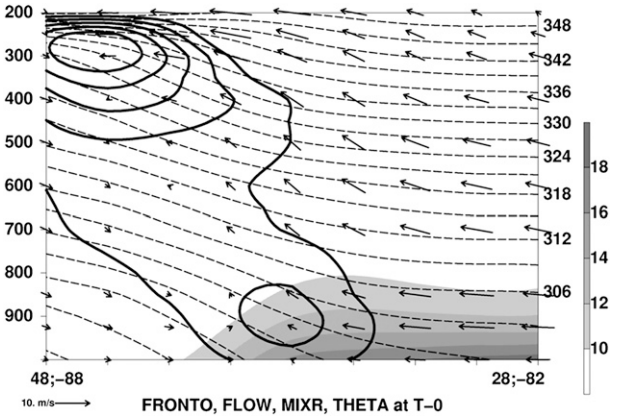

FIG. 9. The AC PRE composite vertical cross section of Petterssen frontogenesis [solid contours every 0.5×10^{-1} K $(100\ \text{km})^{-1}$ $(3\ \text{h})^{-1}$ starting at 0.5×10^{-1} K $(100\ \text{km})^{-1}$ $(3\ \text{h})^{-1}$], potential temperature (dashed contours every 3 K), mixing ratio (shaded according to the grayscale in g kg^{-1}), and flow in the plane of the cross section (arrows in m s^{-1}) at $T - 0$. Cross-section orientation is marked in Fig. 8d.

2) Physical lifting mechanisms

The computation of $\nabla_p \cdot \mathbf{Q}$ at 700 hPa shows that the PRE initiates within a region of 700-hPa QG forcing for ascent east of the composite trough that approaches from the west from $T - 24$ to $T - 0$ (Figs. 8a,c). The forcing for ascent focuses on the southern flank of the 700-hPa thermal gradient. Frontogenesis is indicated, given that the $\mathbf{Q}$ vectors point toward the warmer air in the PRE environment, and is in agreement with the previously inferred deep-layer warm air advection (Fig. 6d). The analysis of 925-hPa equivalent potential temperature θ_e shows a well-defined θ_e ridge that intersects the PRE location by $T - 0$ (Figs. 8b,d). The PRE occurs on the poleward flank of the 925-hPa θ_e ridge in a region of 925-hPa deformation and frontogenesis that becomes organized by $T - 0$ (Figs. 6b,d). A cross section through

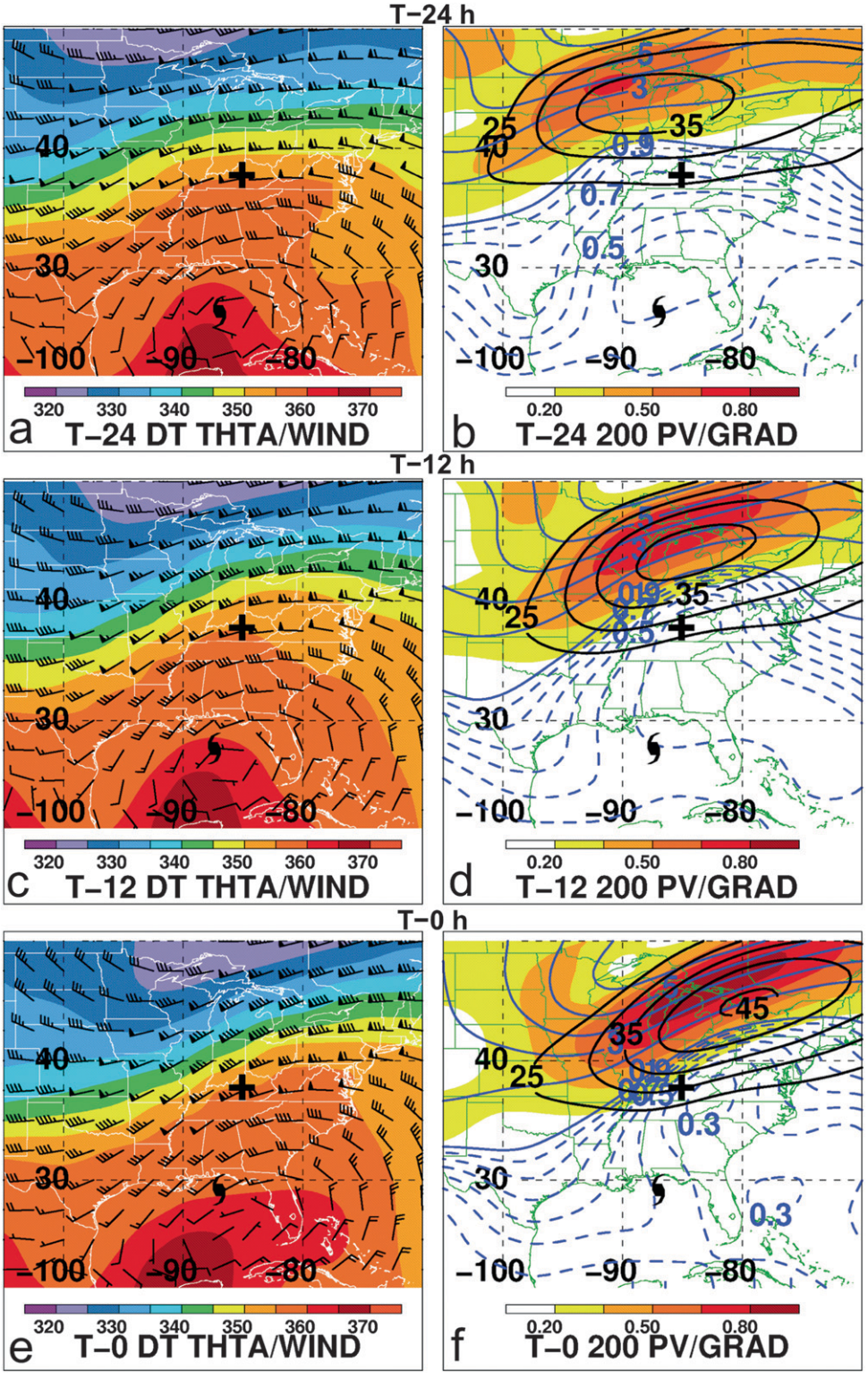

FIG. 10. As in Fig. 6, but for DT potential temperature (shaded according to the color bar in K) and wind (barbs as in Fig. 6) at (a) $T-24$, (c) $T-12$, and (e) $T-0$, and 250–200-hPa PV (solid blue contours every 1.0 PVU starting at 1.0 PVU; dashed blue contours every 0.1 PVU up to 0.9 PVU), layer-average wind speed (solid black contours every 5 m s^{-1} starting at 25 m s^{-1}), and ∇(PV) magnitude (shaded according to the color bar every 0.15×10^{-5} PVU m^{-1}) at (b) $T-24$, (d) $T-12$, and (f) $T-0$. The composite PRE initiation location is marked with a black + symbol and the median parent TC PRE-relative locations are labeled with black TC symbols. 1.0 PVU $\equiv 1.0 \times 10^{-6}$ m^2 s^{-1} K kg^{-1}.

the PRE at $T - 0$ shows that there is deep frontogenesis with relative maxima near 300 and 900 hPa (Fig. 9). Deep ascent is apparent where moist southerly flow intersects the region of deep frontogenesis (Fig. 9). By $T + 24$, forcing for ascent associated with the 700-hPa trough and 925-hPa frontogenesis has moved east of the PRE initiation location, while forcing for ascent directly associated with the TC is beginning to reach the PRE initiation region (Figs. 8e,f).

3) JET INTENSIFICATION THROUGH PRE INITIATION

The intensification of the 200-hPa jet over and northeast of the PRE initiation location from 30 to 45 m s^{-1} between $T - 24$ and $T - 0$ likely increases the broad QG forcing for ascent in the equatorward jet-entrance region (Figs. 6a,c,e). At issue is determining the physical processes that are contributing to upper-level jet intensification in the 24-h period leading up to PRE initiation. To address this issue, dynamic tropopause (DT) and 250–200-hPa potential vorticity (PV) composite analyses are presented in Fig. 10.

At $T - 24$, the PRE initiation location is positioned on the southern flank of a 35 m s^{-1} jet and potential temperature gradient on the DT (Fig. 10a). The composite TC is located beneath a relative minimum in 250–200-hPa PV located south of the PRE initiation location (Fig. 10b). By $T - 0$, the upper-level jet intensified to 45 m s^{-1} as the DT potential temperature gradient increased (note the frontogenesis maximum near 300-hPa in Fig. 9). This jet intensification occurred in response to eastward movement of the upper-level trough to just northwest of the PRE initiation location, and downstream ridge amplification (Figs. 10c,e). The corresponding increase in the 250–200-hPa PV gradient associated with trough and ridge amplification was also likely influenced by the plume of low PV air that moved from over the composite TC at $T - 24$ to just east of the PRE initiation location by $T - 0$ (Figs. 10b,d,f). This result suggests that upper-level jet intensification was likely influenced both by the approach of an upstream trough and TC-related diabatically driven ridge amplification just east of the PRE initiation location.

4. Case analysis of TC Erin PRE of 19 August 2007

a. Overview of case

This section presents a detailed analysis of an AC PRE that occurred in conjunction with TC Erin over the northern Great Plains and Great Lakes region on 19 August 2007 (Table 1 and Fig. 5). Tropical Cyclone Erin formed over the Gulf of Mexico on 15 August 2007,

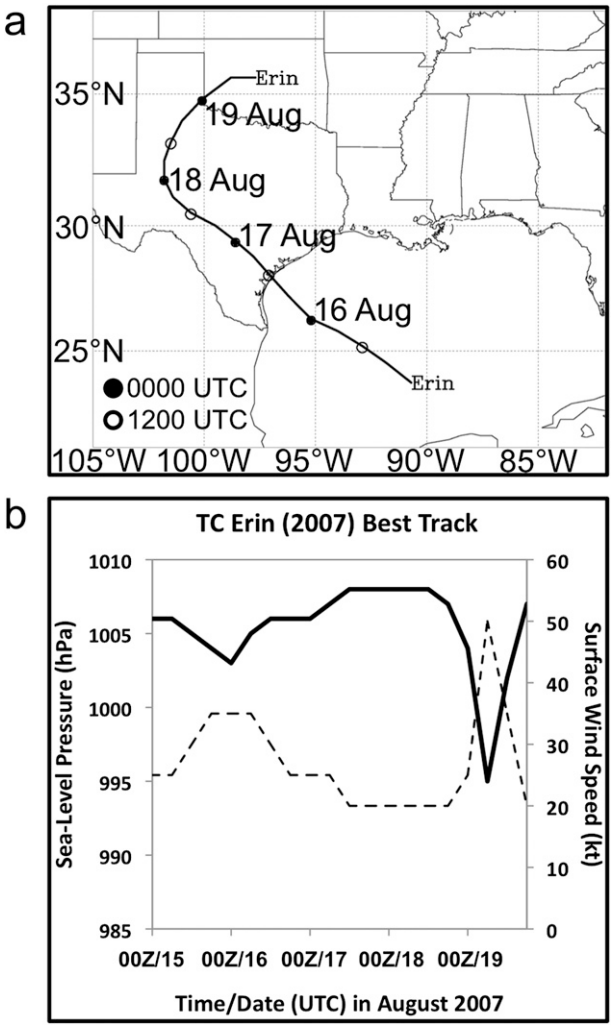

FIG. 11. National Hurricane Center best track (Jarvinen et al. 1984) (a) position, and (b) sea level pressure (solid line in hPa; left axis) and wind speed (dashed line in kt; right axis), for TC Erin (black line) during 15–19 Aug 2007. The 0000 (1200) UTC positions are marked with a(n) (un)filled circle in (a).

made landfall at 1200 UTC 16 August as a weak TS, and subsequently recurved in west Texas into west-central Oklahoma by 0600 UTC 19 August (Figs. 11a,b). In addition to contributing to an AC PRE, TC Erin was most noteworthy for reintensifying to TS strength over Oklahoma on 19 August, nearly 3 days after landfall (Galarneau et al. 2009; Arndt et al. 2009).

The TC Erin PRE began near 2100 UTC 18 August over Minnesota and Wisconsin, expanded eastward to the western shore of Lake Erie, and lasted slightly over 18 h. The separation distance between the remnants of TC Erin and the PRE was approximately 1200 km, and the time lag between PRE initiation and the passage of TC Erin into Illinois was 45 h. The quasi-stationary nature of the deep moist convection in the PRE region

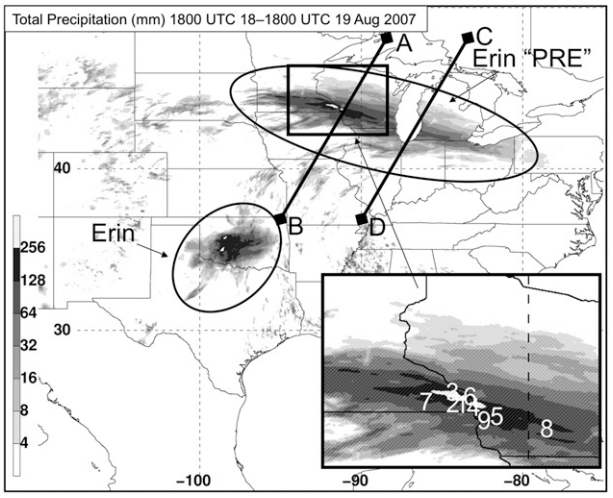

FIG. 12. NPVU QPE analysis (shaded according to the grayscale in mm) for the 24-h period ending 1800 UTC 19 Aug 2007. The positions of TC Erin-related precipitation and TC Erin PRE-related precipitation are labeled with black ovals. The inset shows the region of the PRE with the most intense precipitation. The white numbers on the inset correspond to the stations listed in Table 2. Cross-section orientations (A–B and C–D) for Fig. 18 are also labeled.

resulted in a swath of record rainfall amounts that exceeded 250 mm over Minnesota and Wisconsin (Fig. 12 and Table 2). The resulting widespread severe flooding contributed to seven fatalities and property losses over $170 million (U.S. dollars; NCDC 2007).

b. Physical mechanisms driving heavy rainfall

The synoptic analysis for initiation time of the TC Erin PRE—0000 UTC 19 August—is shown in Fig. 13 for comparison with the AC PRE composite (Figs. 6 and 8). The TC Erin PRE initiated in the equatorward jet-entrance region of a 60 m s^{-1} 200-hPa jet (Fig. 13a). Beneath the jet-entrance region a southerly feed of deep tropical moisture, with PW values >52 mm, intersected a low-level baroclinic zone that stretched eastward from a developing lee cyclone over western South Dakota to Lake Michigan (Figs. 13b,d). The moisture plume was also depicted in the NOAA blended TPW product in the 36-h period leading up to 0600 UTC 19 August (Kusselson et al. 2009, see their Fig. 6). The PW and low-level moisture flux in the TC Erin moisture plume was characterized by normalized anomalies (Hart and Grumm 2001) of 2.0–3.0 standard deviations above normal (M. Brennan 2008, personal communication). The TC Erin PRE was situated within a region of 700-hPa QG forcing for ascent over Minnesota, Wisconsin, and Iowa along the equatorward flank of the baroclinic zone (Fig. 13c). With the **Q** vectors pointing toward the warmer air where the PRE formed, low-level frontogenesis was likely important in focusing vigorous ascent along the baroclinic zone on the northern flank of 925-hPa θ_e ridge (Figs. 13c,d). The synoptic-scale conditions at the time of initiation of the TC Erin PRE are quite similar to the AC PRE composite at $T - 0$.

Radar imagery showed that an area of eastward-moving precipitation stretched from southeast Minnesota to northern Illinois at 1800 UTC 18 August (Fig. 14a). The precipitation became better organized by 0000 UTC 19 August as a narrow convective line formed on the western flank of the rain shield over southern Minnesota (Figs. 14b,c). As the individual convective cells moved eastward within the broad PRE rain shield, new cells continuously formed on the western flank of the PRE through 0900 UTC 19 August (Figs. 14c–f). This new back-building convection and the associated training echoes resulted in a nearly stationary MCS along and north of the surface baroclinic zone that stretched from South Dakota through Iowa into southern Illinois. North of the boundary, westerly 0–6-km wind shear values approached 30 m s^{-1}. The strong westerly shear north of the baroclinic zone set the stage for a classic "frontal" flash flood as described by Maddox et al. (1979) and others, and for the training line/adjoining stratiform mode of MCS organization described by Schumacher and

TABLE 2. Selected rainfall totals (mm) during the TC Erin (2007) PRE. The number of the rainfall total listing corresponds to the numbers labeled on Fig. 12. Automated surface observing system station (ASOS) and National Weather Service cooperative observer program station (COOP).

Station	Type	Precipitation (mm)	Time period
1. Hokah, MN	COOP	383.5	24-h period ending 1300 UTC 19 Aug
2. Houston, MN	COOP	529.6	18–20 Aug
3. Witoka, MN	COOP	431.8	18–19 Aug
4. Stoddard, WI	COOP	315.2	18–19 Aug
5. Lone Rock, WI	ASOS	160.0	24-h period ending 1800 UTC 19 Aug
6. La Crosse, WI	ASOS	136.4	24-h period ending 1800 UTC 19 Aug
7. Rochester, MN	ASOS	131.3	24-h period ending 1800 UTC 19 Aug
8. Madison, WI	ASOS	125.9	24-h period ending 1800 UTC 19 Aug
9. Boscobel, WI	ASOS	106.9	24-h period ending 1800 UTC 19 Aug

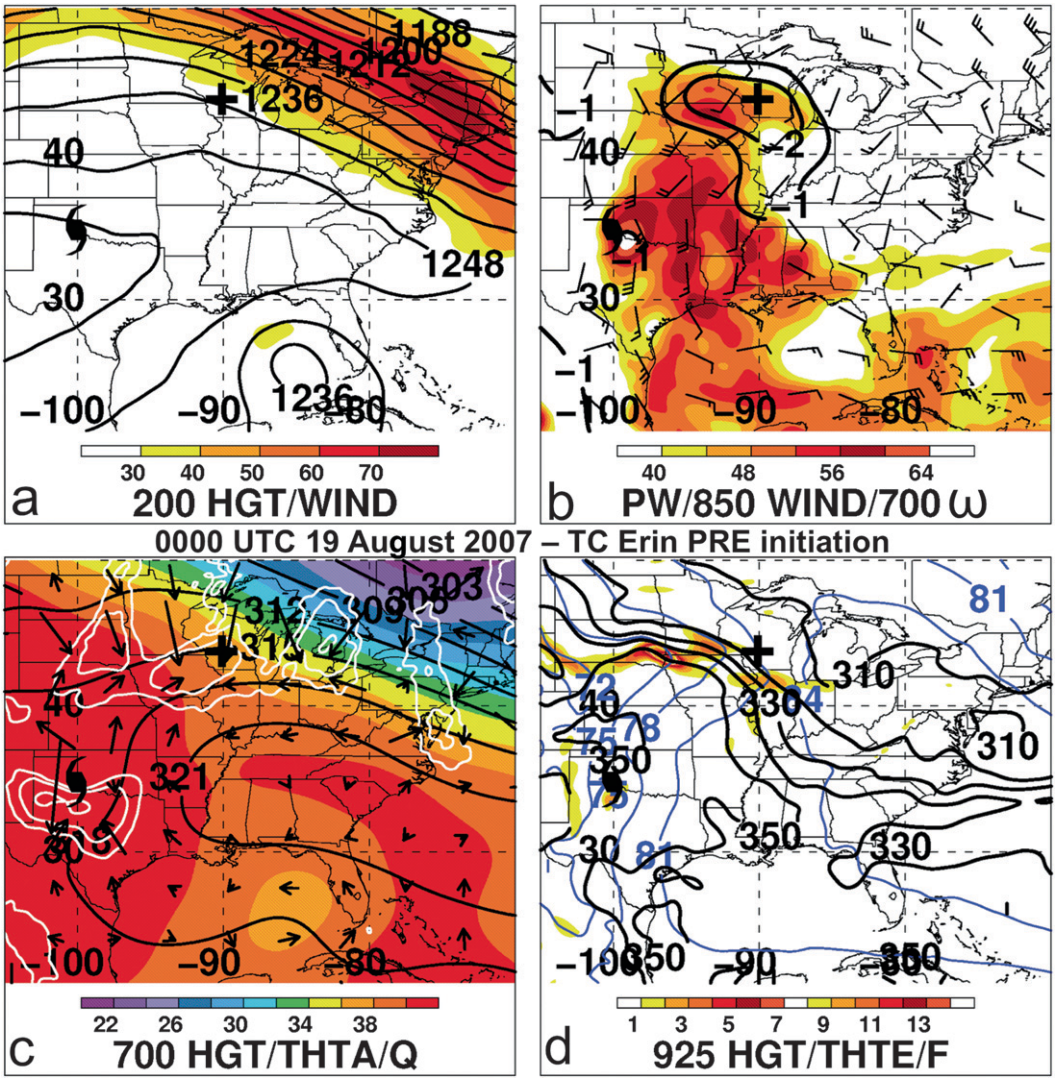

FIG. 13. The NCEP GFS analysis of (a) 200-hPa geopotential height (solid contours every 6 dam) and wind speed (shaded according to the color bar in m s^{-1}); (b) total column PW (shaded in mm), 700-hPa vertical motion (upward motion in black contours every 1.0×10^{-3} hPa s^{-1} starting at -1.0×10^{-3} hPa s^{-1}), and 850-hPa wind (barbs as in Fig. 6); (c) 700-hPa geopotential height (solid contours every 3 dam), potential temperature (shaded according to the color bar in °C), **Q** vectors (arrows in 10^{-8} Pa m^{-1} s^{-1}), and $-\nabla\cdot\mathbf{Q}$ (white contours every 3.0×10^{-12} K m^{-2} s^{-1} starting at 3.0×10^{-12} Pa m^{-2} s^{-1}); and (d) 925-hPa geopotential height (thin blue contours every 3 dam), equivalent potential temperature (thick black contours ≤350 K every 10 K), and Petterssen frontogenesis [shaded according to the color bar in K (100 km)$^{-1}$ (3 h)$^{-1}$] at 0000 UTC 19 Aug 2007. The PRE initiation location is marked with a black + symbol and TC Erin with a black TC symbol.

Johnson (2005). The PRE was most intense at 0600 UTC 19 August when cloud top temperatures <-70°C were apparent in infrared satellite imagery (Fig. 15). This satellite imagery also illustrates the difference in convective structure between TC Erin and the PRE, with the former being a quasi-circular convective system and the latter a quasi-linear convective system. This difference in convective structure between the PRE and parent TC is a common signature among the 17 AC PREs in the composite dataset. A manual surface analysis of θ and mixing ratio at 0600 UTC 19 August reveals that the PRE convection continuously developed just north of the surface baroclinic zone over southern Minnesota; directly north of where surface moisture (mixing ratio values near 18 g kg^{-1}) was maximized on the south side of the baroclinic zone over western Iowa (Fig. 16).

The organization of the PRE during the 12-h period leading up to 0600 UTC 19 August coincided with a

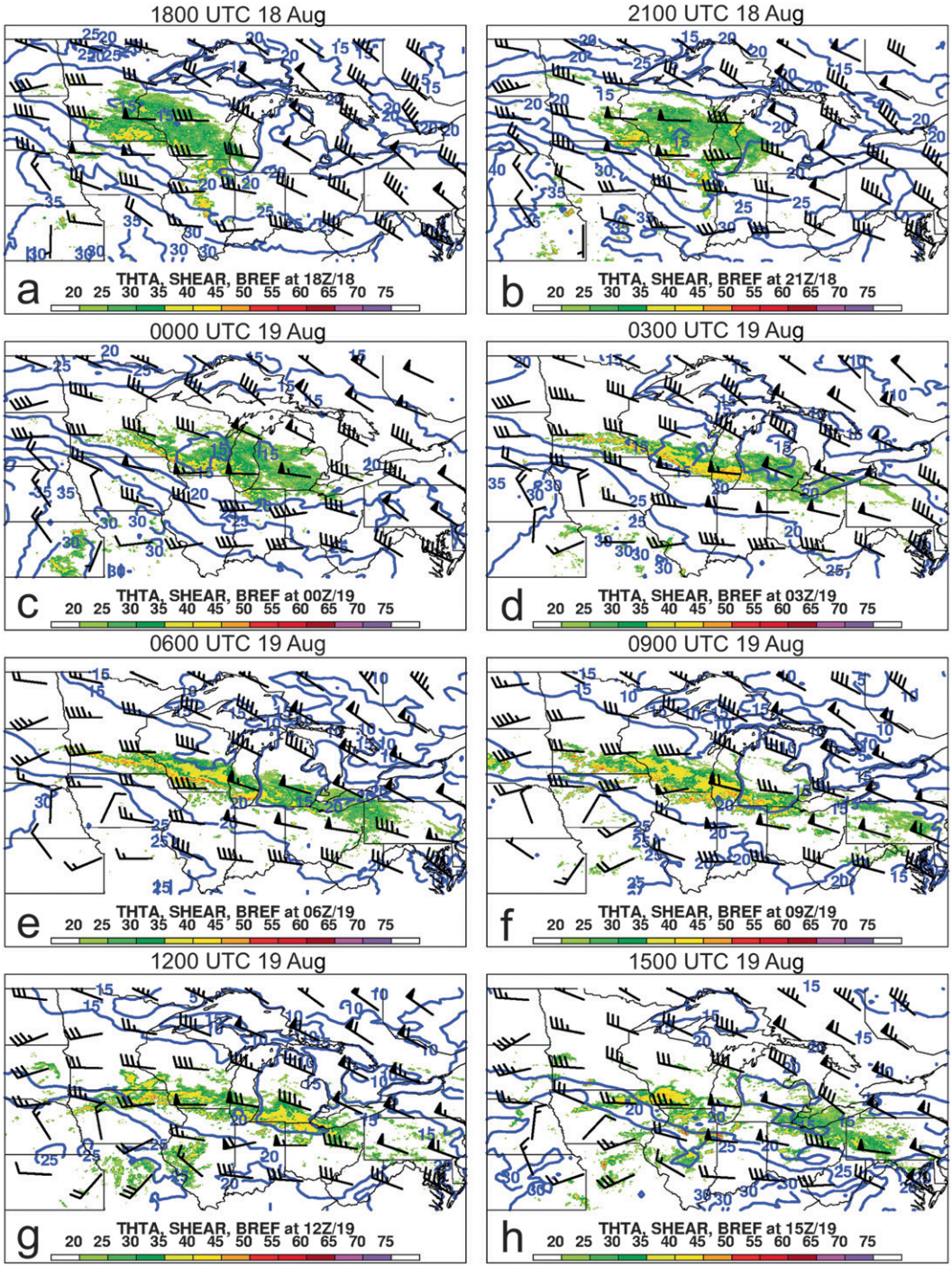

FIG. 14. RUC analyses of 2-m potential temperature (solid blue contours every 5°C), and 0–6-km wind shear (barbs as in Fig. 6) are overlaid on a WSR-88D base reflectivity data mosaic (shaded according to the color bar in dB*Z*) at (a) 1800 UTC 18 Aug, (b) 2100 UTC 18 Aug, (c) 0000 UTC 19 Aug, (d) 0300 UTC 19 Aug, (e) 0600 UTC 19 Aug, (f) 0900 UTC 19 Aug, (g) 1200 UTC 19 Aug, and (h) 1500 UTC 19 Aug 2007.

notable increase in the 850-hPa frontogenesis along the northwest–southeast-oriented baroclinic zone stretching from South Dakota to southern Illinois and Indiana (Figs. 17a–c). By 0600 UTC 19 August, a maximum in 850-hPa frontogenesis was in place over southeast Minnesota and southern Wisconsin, where the heaviest PRE rainfall rates were observed. The organization of the frontogenesis in the PRE region occurred in

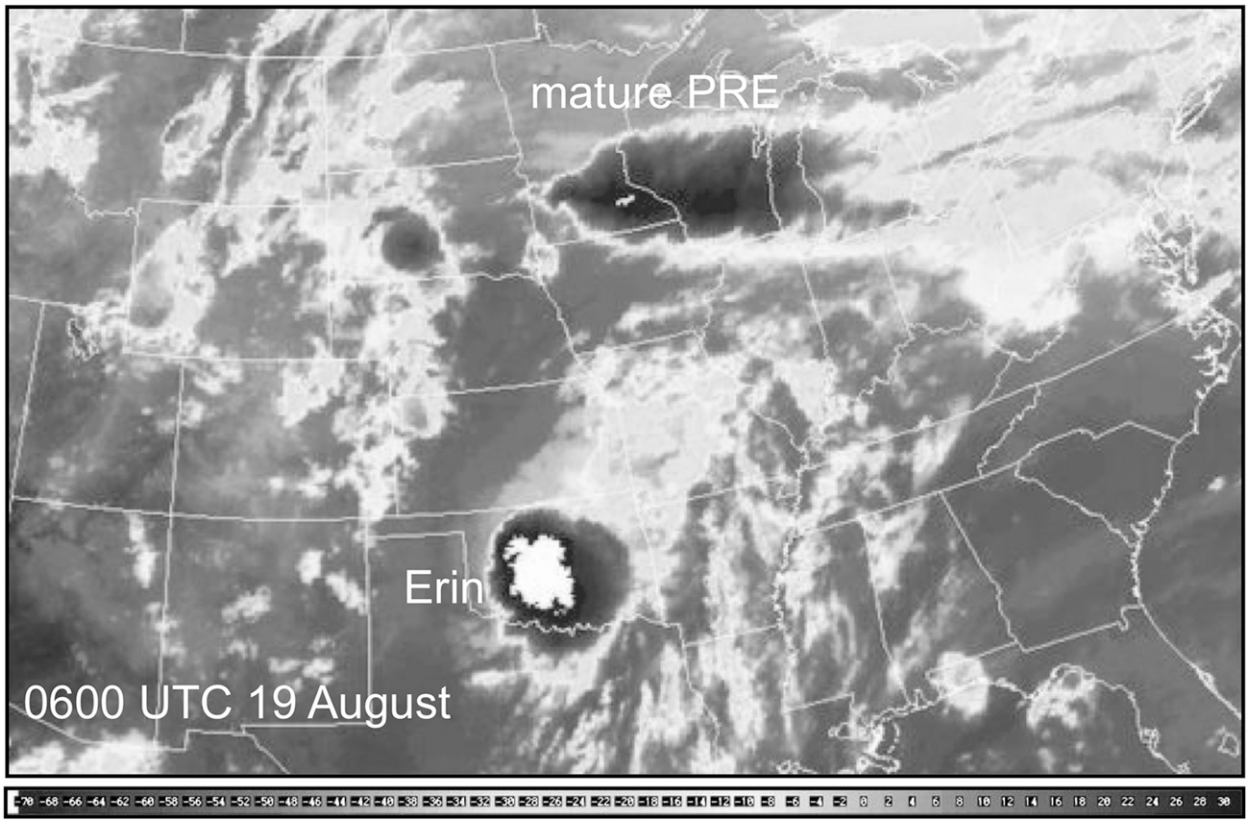

FIG. 15. *GOES-12* infrared image (shaded according to the grayscale in °C) at 0600 UTC 19 Aug 2007. TC Erin and the PRE cloud shields are labeled.

response to the observed strengthening of the low-level jet that reached 15–20 m s^{-1} and was oriented perpendicular to the baroclinic zone (Fig. 17c). By 1200 UTC 19 August, the PRE and 850-hPa frontogenetical forcing weakened (Figs. 14g and 17d). The frontogenesis weakened in response to nocturnal cooling on the south side of the baroclinic zone, and veering of the low-level jet that resulted in the flow being oriented more parallel to the frontal zone (Figs. 17c,d). By 1500 UTC 19 August, a small remaining region of deep moist convection was located over southern Wisconsin as the PRE continued to dissipate (Fig. 14h).

Vertical cross sections through the most intense region of the PRE (sections A–B) and farther east (sections C–D) at 0600 and 1200 UTC 19 August show the importance of low-level frontogenesis in focusing vigorous low-level ascent during the mature stage of the PRE (Figs. 18a,b). During the mature stage of the PRE at 0600 UTC 19 August a deep moist southerly flow (mixing ratio values near 18 g kg^{-1}) was lifted along the baroclinic zone in a region of low-level frontogenesis (Fig. 18a). Farther east the ascent was weaker especially at lower levels likely from the low-level flow being oriented more parallel to the frontal zone, which contributed to weaker frontogenetical forcing (Fig. 18b). Precipitation was less organized at 1200 UTC 19 August than 6 h earlier (Fig. 14g) in response to weaker frontogenetical forcing (Figs. 17c,d) despite ample low-level moisture still in place (Fig. 18c) and increased moisture farther east along cross sections C–D (Fig. 18d).

c. Evolution of TC Erin moisture

While adequate synoptic and mesoscale forcing was in place, and record rainfall amounts were observed, the remaining condition required to qualify this heavy rain event as a PRE was the transport of deep tropical moisture northward from TC Erin to the PRE. At 0000 UTC 16 August, TC Erin was embedded in a plume of deep tropical moisture, with PW values >60 mm just off the Texas coast 12 h prior to landfall (Fig. 19a). Farther north, an ambient zonally oriented region of enhanced moisture, with PW values ranging from 35 to 50 mm, was located south of a baroclinic zone (left behind from a previous extratropical cyclone) on the poleward flank of a 700-hPa anticyclone. Note that PW values within this ambient moisture region at Omaha, Nebraska, reached

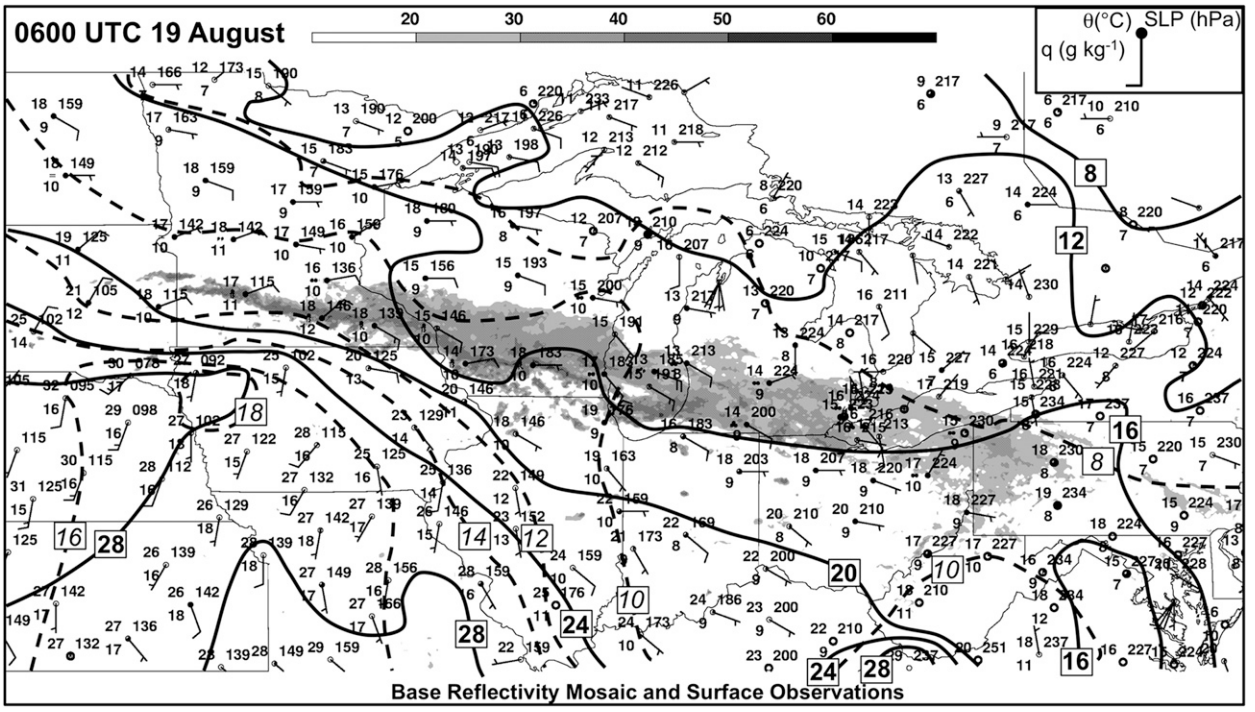

FIG. 16. Manual analysis of surface potential temperature (solid black contours every 4°C) and mixing ratio (dashed contours every 2.0 g kg^{-1}) overlaid on a WSR-88D base reflectivity mosaic (shaded according to the grayscale in dBZ) at 0600 UTC 19 Aug 2007. Surface potential temperature θ, mixing ratio q, and sea level pressure (SLP) are plotted on the surface station models as shown in the inset on the upper-right part of the figure.

48 mm on 16 August (Fig. 20). Tropical Cyclone Erin continued to move northwestward on the southwest flank of the 700-hPa anticyclone, and by 0000 UTC 17 August was located over the Texas hill country (Fig. 19b). By 0000 UTC 18 August, the moisture plume associated with TC Erin began to surge northward in the strengthening southerly flow on the western flank of the 700-hPa anticyclone (Fig. 19c), with PW values reaching 50 mm at Haskell, Oklahoma (Fig. 20). The 700-hPa southerly flow increased in response to the increasing height gradient between TC Erin and the strengthening ridge over the southeast United States. Furthermore, the western part of the moisture region near the remnant baroclinic zone on the poleward side of the anticyclone began to move north in response to increased southerly flow over Colorado and eastern Nebraska east of a developing lee trough (Fig. 19c and 20).

By 0000 UTC 19 August, the TC Erin moisture plume surged into northern Missouri and extreme southern Iowa in response to 10–15 m s^{-1} southerly flow at 850 and 700 hPa (Figs. 17b and 19d), but remained distinct from the ambient moisture that was now situated over northern Iowa. The PW values at Hillsboro, Kansas, and Topeka, Kansas, rapidly increased to near 55 mm in response to the poleward surge of Erin moisture (Fig. 20). The rainfall that extended from Minnesota to Lake Michigan was already becoming organized by 0000 UTC 19 August, prior to the arrival of the TC Erin moisture, suggesting that there would have been rainfall in that area whether TC Erin moisture was present or not (Fig. 14c). By 0600 UTC 19 August, the TC Erin moisture plume and the ambient moisture merged over the PRE region (Figs. 19e and 20; see also Fig. 6 in Kusselson et al. 2009). This merged moisture plume surged eastward into Illinois, Indiana, and Michigan by 1200 UTC 19 August (Fig. 19f). Atmospheric soundings from Davenport, Iowa (DVN), and Lincoln, Illinois (ILX), at 0000 and 1200 UTC 19 August show the large increase in total column PW as the TC Erin moisture plume surged northward to the PRE region (Fig. 21). The DVN and ILX PW values increased from 40 and 41 mm, respectively, at 0000 UTC to 50 and 55 mm, respectively, at 1200 UTC 19 August. This increase in PW produced nearly moist adiabatic conditions through a deep layer, which likely limited the production of convectively driven deep cold pools and contributed to the quasi-stationary nature of the PRE convective system. The soundings also indicate the presence of deep westerly quasi-unidirectional flow above 900 hPa, which is consistent with the observed training and back-building

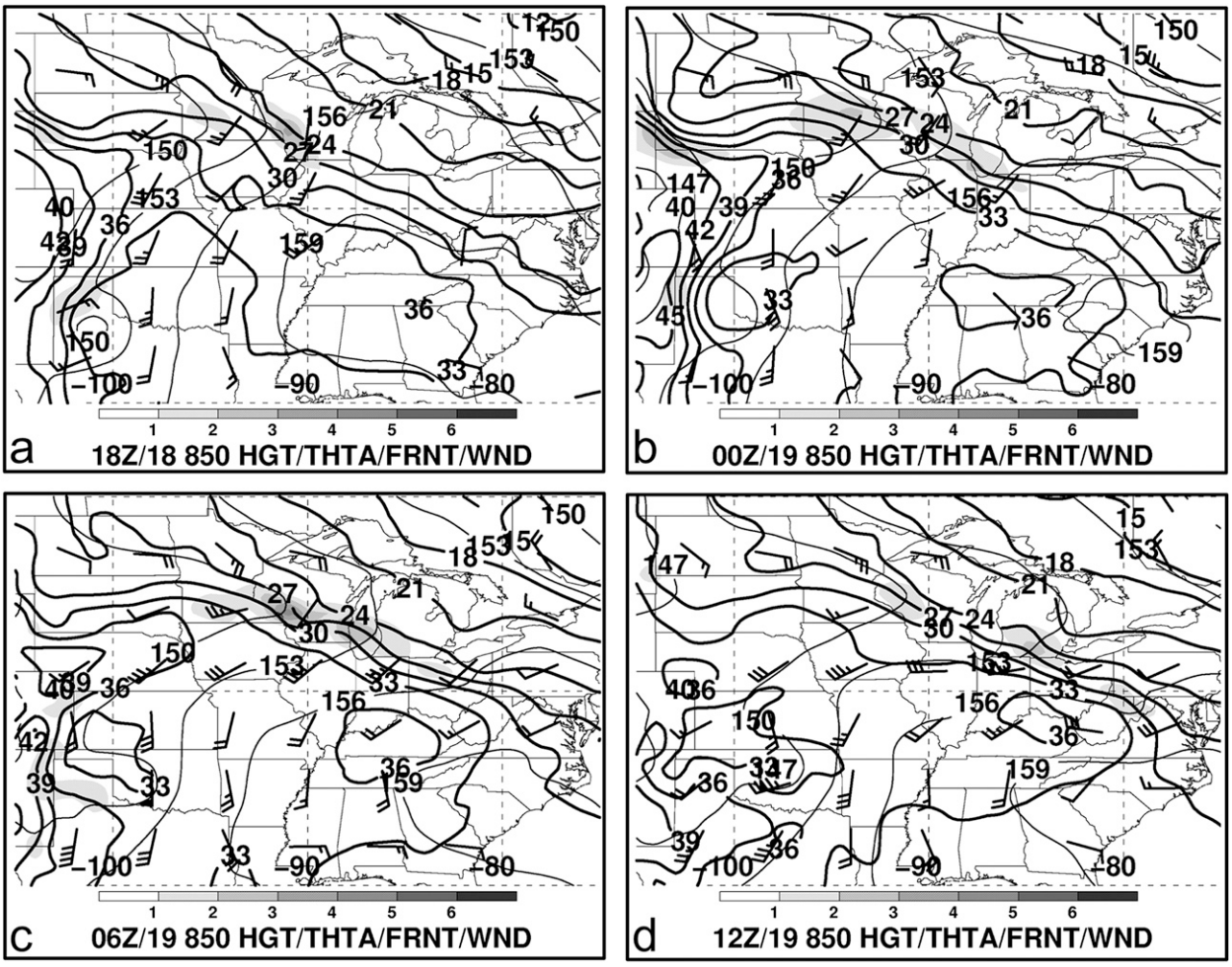

FIG. 17. The 850-hPa geopotential height (solid thin contours every 3 dam), wind (barbs as in Fig. 6 $\geq$7.5 m s^{-1}), potential temperature (solid thick contours every 3°C), and 900–800-hPa layer-averaged Petterssen frontogenesis [shaded according to the grayscale in °C (100 km)$^{-1}$ (3 h)$^{-1}$] at (a) 1800 UTC 18 Aug, (b) 0000 UTC 19 Aug, (c) 0600 UTC 19 Aug, and (d) 1200 UTC 19 Aug 2007.

behavior of the convective cells in the strong westerly wind shear north of the surface baroclinic zone (Figs. 14c–g).

To establish the source of the deep tropical moisture in the PRE region, 20 backward air parcel trajectories beginning at 0600 UTC 19 August in the PRE region are shown in Fig. 22. These air parcel trajectories, overlaid on the PW analysis at 0600 UTC 16 August, show that the air parcels have four distinct source regions based on their position at 0600 UTC 16 August: north of the baroclinic zone over southern Canada (1 of 20 air parcel trajectories), just south of the baroclinic zone over northwest Missouri and southeast Nebraska (3 of 20), within the TC Erin moisture plume over the Gulf of Mexico (11 of 20), and over the southeast United States (5 of 20; Fig. 22a). Time series of the median air parcel pressure (Fig. 22b) for each of the four source regions indicate that all air parcels ascended as they approached the PRE region, which agrees with the isentropic ascent along the low-level baroclinic zone inferred from Fig. 18a. The median relative humidity time series shows how the air parcels within the TC Erin plume remained moist, with values above 70%, 48–72 h prior to reaching the PRE region when compared to the other 3 source regions that had values near 50%–60% prior to 0000 UTC 18 August (Fig. 22c). This relatively high moisture indicates that the air within the TC Erin moisture plume was particularly moist as compared to surrounding regions, and further shows that the TC Erin moisture arrived in the PRE region prior to the mature phase of the MCS at 0600 UTC 19 August.

d. Forecasting postscript

Given the difficult quantitative precipitation forecasting (QPF) challenge and large societal impacts that PREs can pose (Fig. 1), and the unprecedented rainfall

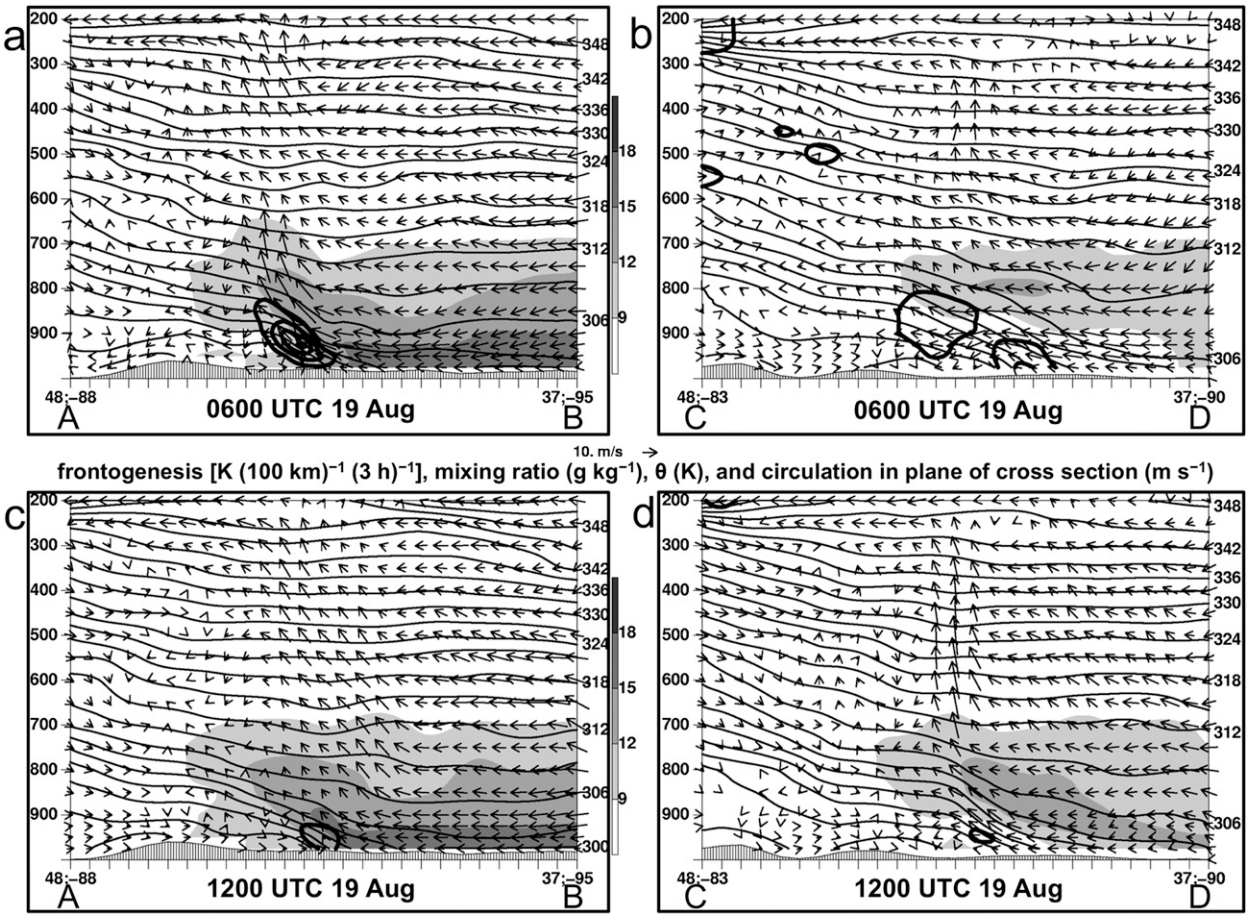

FIG. 18. Vertical cross section of mixing ratio (shaded according to the grayscale in g kg^{-1}), potential temperature (thin solid contours every 3 K), Petterssen frontogenesis [thick solid contours every 2.0°C (100 km)$^{-1}$ (3 h)$^{-1}$ starting at 2.0°C (100 km)$^{-1}$ (3 h)$^{-1}$], and flow in the plane of the cross section (arrows in m s^{-1}; reference vector in center of four-panel diagram) at (a),(b) 0600 and (c),(d) 1200 UTC 19 Aug 2007. Cross-section orientations are labeled in Fig. 12.

amounts that occurred with the TC Erin PRE, it is of interest to briefly examine the forecast performance for this event. Figure 23 shows the European Centre for Medium-Range Weather Forecasts (ECMWF) ensemble prediction system (EPS) 48-h precipitation forecasts initialized at various times leading up to the TC Erin PRE. The ECMWF EPS (Buizza et al. 2007) data was obtained from The Observing System Research and Predictability Experiment (THORPEX) Interactive Grand Global Ensemble (TIGGE) archive, and has 51 members with a spectral truncation of T399 (corresponding to approximately 50-km horizontal grid spacing) and 62 vertical levels.

Perhaps the most striking aspect of the ECMWF EPS probability of precipitation (POP) forecasts is the consistent indication that a heavy rain event could occur over Minnesota and Wisconsin during the 48-h period ending 1200 UTC 20 August from forecasts as early as 1200 UTC 14 August (Fig. 23). The POP 96–144-h forecast initialized at 1200 UTC 14 August indicated a 30% chance of ≥50 mm of rainfall over southwest Wisconsin, northeast Iowa, and southeast Minnesota (Fig. 23c). The forecasted area of heavy rainfall became more focused over southern Minnesota and Wisconsin during subsequent 1200 UTC forecast cycles, with an elongated region of 90% POP ≥50 mm emerging in the 0–48-h forecast initialized at 1200 UTC 18 August (Figs. 23a–c). The favorable performance of the ECMWF EPS POP forecasts for the TC Erin PRE may in part be related to the quasi-stationary nature of the low-level baroclinic zone over the northern Great Plains and Great Lakes region, which provided the primary forcing mechanism for the heavy rainfall.

Despite the poor forecasts of the TC Erin vortex track (not shown), the EPS still indicated that a heavy rain event would occur over the northern Great Plains and Great Lakes region in the 48-h period ending 1200 UTC 20 August (Fig. 23). This result suggests that there would

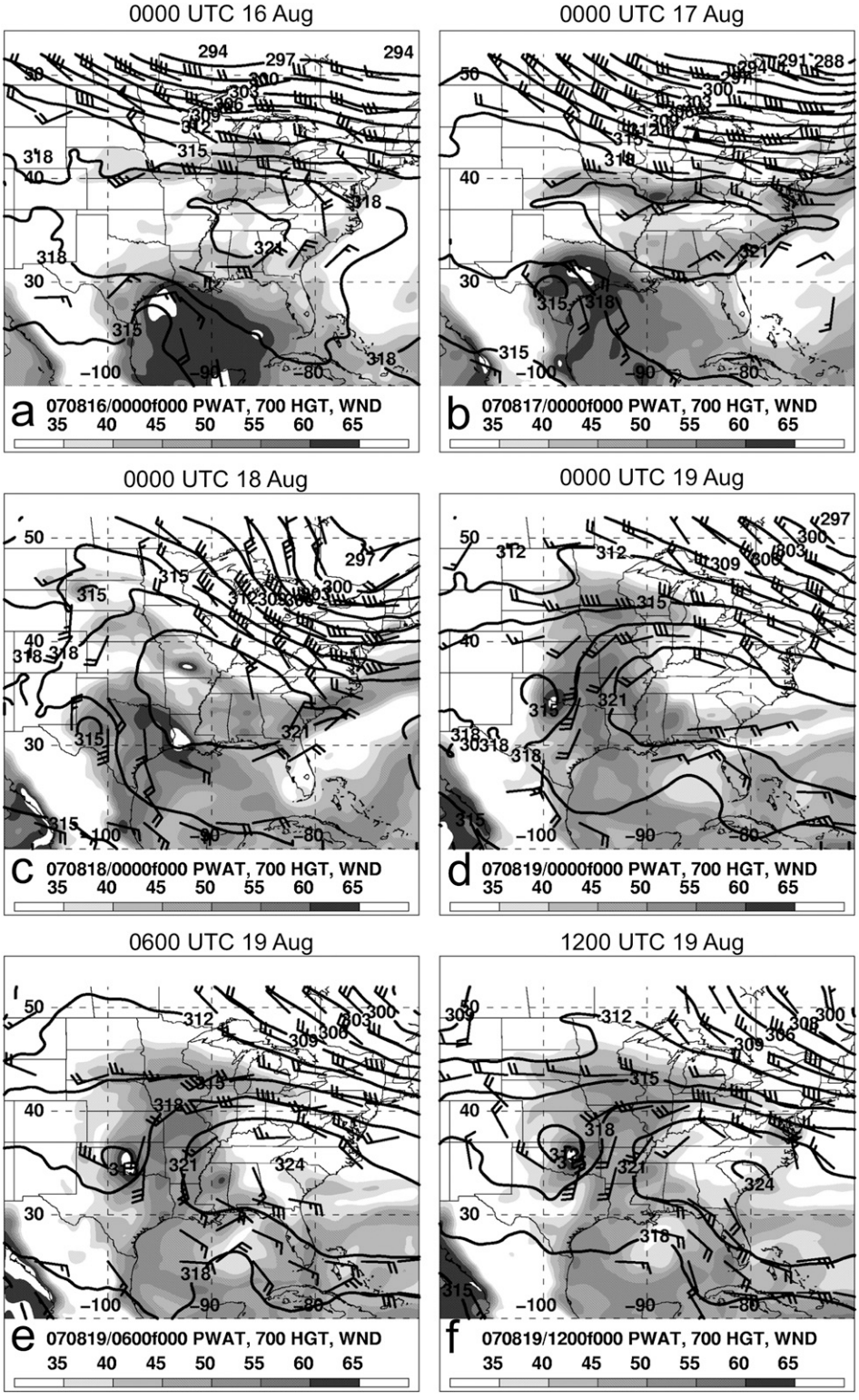

FIG. 19. The 700-hPa geopotential height (solid contours every 3 dam), wind (barbs as in Fig. 6 $\geq$10 m s^{-1}), and total column PW (shaded according to the grayscale in mm) at (a) 0000 UTC 16 Aug, (b) 0000 UTC 17 Aug, (c) 0000 UTC 18 Aug, (d) 0000 UTC 19 Aug, (e) 0600 UTC 19 Aug, and (f) 1200 UTC 19 Aug 2007.

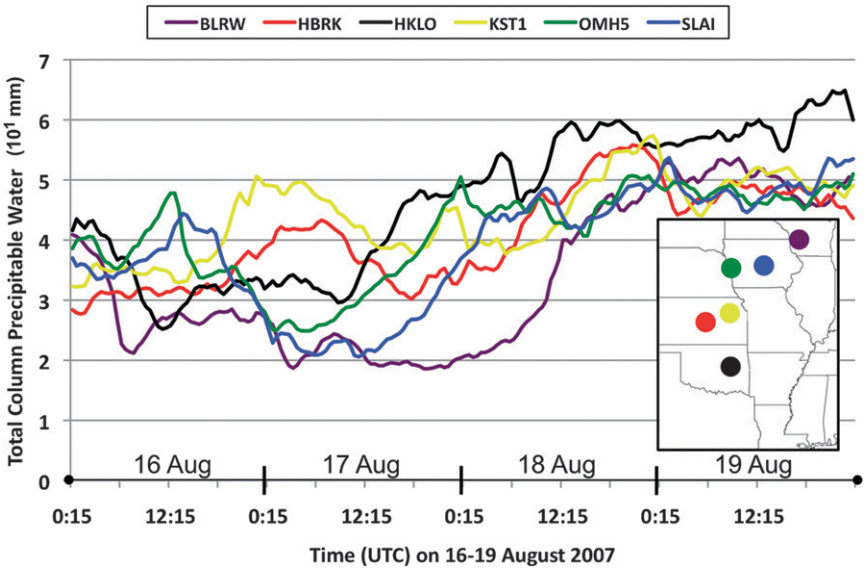

FIG. 20. Time series of NOAA/GSD GPS-Meteorology Observing System total column precipitable water (×10 mm) for 16–19 Aug 2007 at Blue River, WI (BLRW; purple), Slater, IA (SLAI; blue), Omaha, NE (OMH5; green), Topeka, KS (KST1; yellow), Hillsboro, KS (HBRK; red), and Haskell, OK (HKLO; black).

have been a significant heavy rain event over the northern Great Plains and upper Midwest regardless of the track and behavior of TC Erin. It is likely, however, that the deep tropical moisture associated with TC Erin turned what would have been a notable rain event, into a historical record-breaking 2000-yr rain event as estimated by the Minnesota State Climate Office (see online at http://climate.umn.edu/doc/journal/flash_floods/ff070820.htm).

5. Conclusions

This paper represents the first known systematic multiscale study of PREs. A synoptic climatology of PREs that occurred during 1995–2008 east of the Rockies in association with North Atlantic TCs and a detailed case study of the TC Erin PRE from 19 August 2007 were presented.

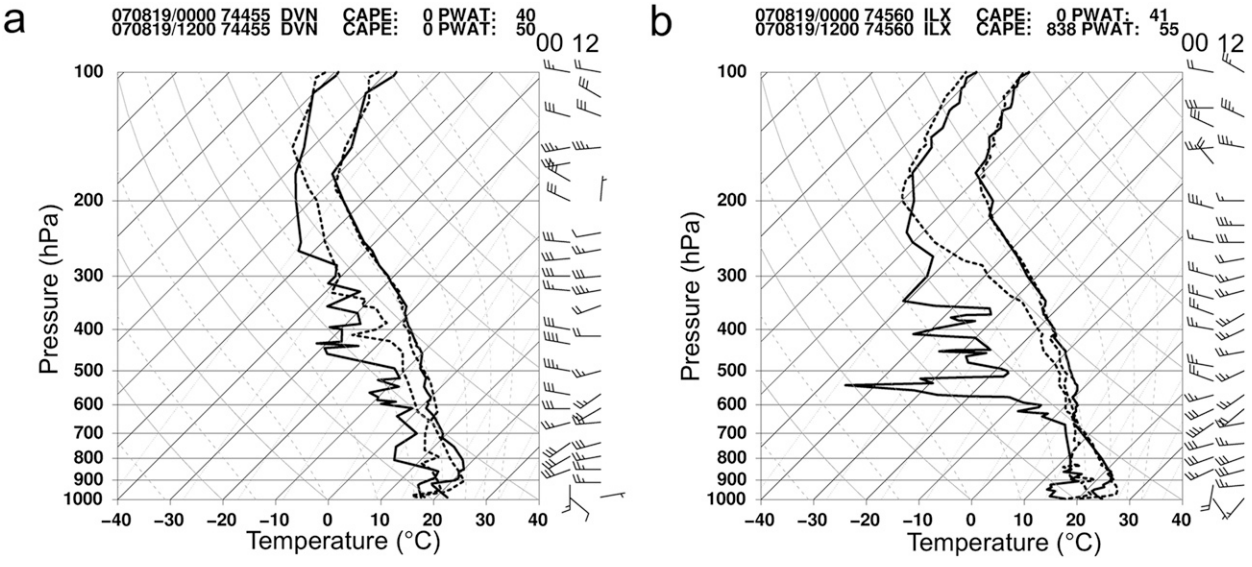

FIG. 21. Skew T–log$p$ diagram of air temperature (°C), dewpoint (°C), and wind (barbs as in Fig. 6) at 0000 (solid lines) and 1200 (dashed lines) UTC 19 Aug 2007 for (a) Davenport, IA (DVN), and (b) Lincoln, IL (ILX). CAPE (J kg^{-1}) and total column PW (PWAT; mm) are labeled at the top of (a),(b).

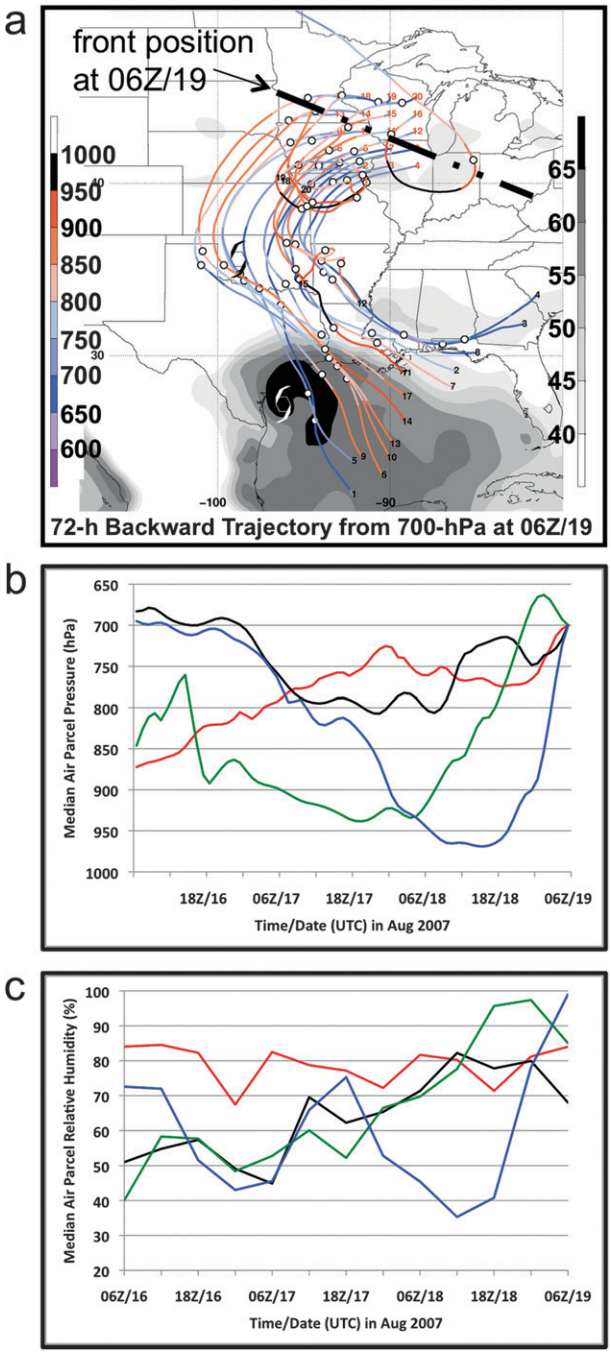

FIG. 22. (a) Twenty 72-h backward air parcel trajectories beginning at 700 hPa at 0600 UTC 19 Aug 2007. The numbers identify individual air parcel trajectories, while the circles mark 0000 UTC positions. The air parcel pressure values are indicated by the contour color (according to the left color bar in hPa). The air parcel trajectories are overlaid on the 0600 UTC 16 Aug 2007 analysis of total column PW (shaded according to the right grayscale in mm). The position of TC Erin at 0600 UTC 16 Aug and 0600 UTC 19 Aug 2007 are labeled by white and black tropical storm symbols, respectively, while the 0600 UTC 19 Aug 2007 position of the synoptic front is labeled with a dash–dot–dot contour. The median air parcel (b) pressure (hPa) and (c) relative humidity (%) for air parcels originating within the TC Erin moisture plume (red), over the southeast United States east of the TC Erin moisture plume (black), north of the synoptic front (blue), and just south of the synoptic front within the ambient moisture plume (green) are also shown.

The synoptic climatology showed that approximately 30% of all TCs that passed west of 70°W and north of 20°N produced at least 1 PRE, and that PREs occurred most frequently in August and September. Although PREs can occur with TCs of all intensities, they occur most commonly with strong TCs that reach a maximum intensity of at least category 3. This result suggests the possibility that TC intensity may influence the potential for PRE occurrence, likely by providing more widespread deep tropical moisture or by intensifying the downstream upper-level jet through diabatically forced ridge amplification. The median PRE–TC separation distance, time lag, and longevity among the PRE categories were approximately 1000 km, 36 h, and 15 h, respectively. These statistics provide climatological guidelines for forecasters to anticipate where in relation to the TC a PRE will occur, how long in advance of the TC the PRE will occur, and how long the PRE will last.

The composite synoptic-scale environment for AC PREs exhibits notable similarity to the schematic for antecedent heavy rainfall ahead of TC Agnes (1972) provided by Bosart and Carr (1978, see their Fig. 2). Cote (2007) revised and updated the Bosart and Carr (1978) schematic for LOT PREs in advance of TCs (Fig. 24), which is also applicable to and succinctly summarizes the AC PRE composites shown in Figs. 6–10. On the synoptic scale, PREs form in the equatorward jet-entrance region of a 200-hPa jet, on the western flank of a 925-hPa θ_e ridge just east of a 700-hPa midlatitude trough (Fig. 24a). On the mesoscale, a low-level baroclinic zone can act to focus heavy rainfall through frontogenetical forcing beneath the equatorward jet-entrance region of the 200-hPa jet (Fig. 24b). The schematic also suggests that orography can act as a mesoscale focusing mechanism for heavy precipitation in regions of upslope flow as previously documented by Bosart and Carr (1978) and Srock and Bosart (2009).

Examination of individual cases has shown that AC PREs frequently behave like the Maddox et al. (1979) frontal-type flash flooding MCS events. One such example was presented in this paper as a case study of the TC Erin PRE of 19 August 2007. The TC Erin PRE produced widespread flooding rainfall over southern Minnesota and Wisconsin on 19 August 2007. This PRE

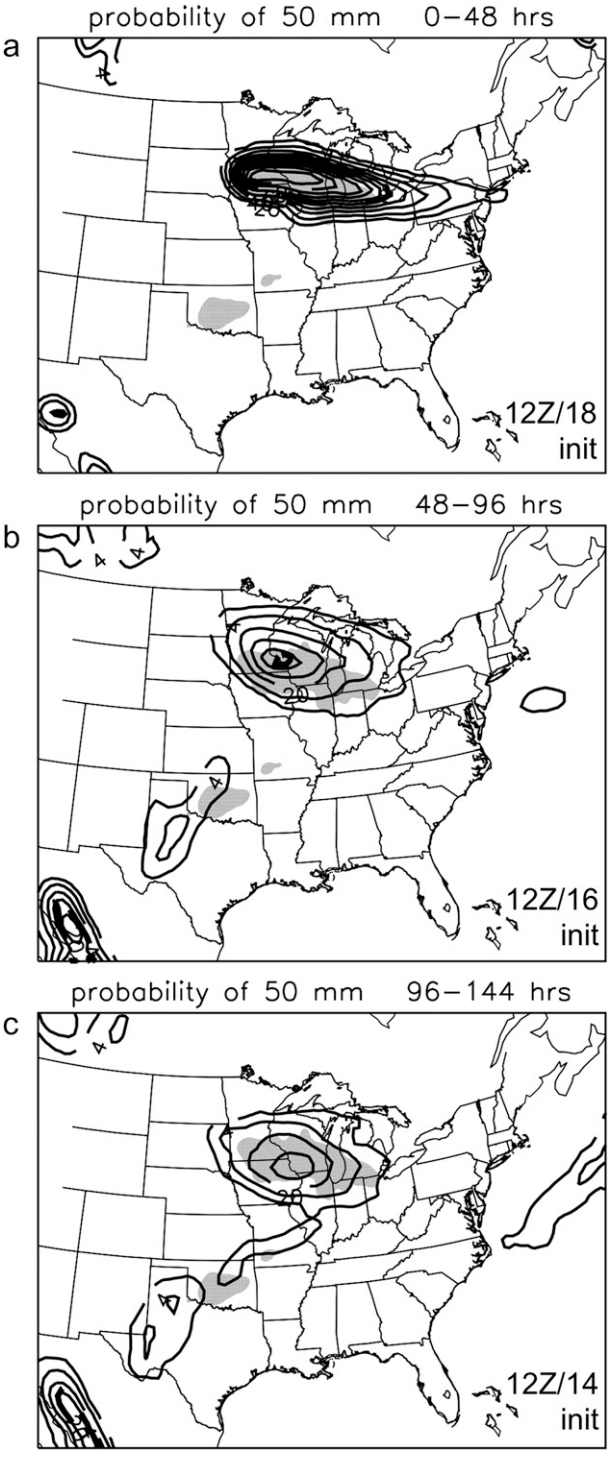

FIG. 23. Raw ECMWF EPS probabilities, at increasing lead times, of 50 mm of precipitation in the 48-h period between 1200 UTC 18 Aug and 1200 UTC 20 Aug 2007. Probabilities are contoured at 4% (i.e., approximately 2 ensemble members), 10% and every 10% above that. Areas where at least 50 mm of precipitation was observed are shaded in gray. The 48-h precipitation totals are simply the sum of the two 24-h totals ending 1200 UTC 19 Aug and 20 Aug 2007, and were subsequently filtered with a 3-point smoother for readability. Model initialization times shown are 1200 UTC (a) 18 Aug, (b) 16 Aug, and (c) 14 Aug 2007. (The NOAA/Climate Prediction Center U.S. Daily Precipitation Analysis data can be found online at ftp://ftp.cpc.ncep.noaa.gov/precip/wd52ws/us_daily/.)

occurred in a region of focused low-level ascent over and north of a quasi-stationary surface baroclinic zone and beneath a 200-hPa equatorward jet-entrance region. A slow-moving MCS formed just north of this baroclinic zone, in an environment of strong westerly wind shear, and resembled the Maddox et al. (1979) and Schumacher and Johnson (2005) frontal-type heavy-rain-producing MCS. The maturation of the TC Erin PRE MCS by 0600 UTC 19 August occurred in response to (i) increased low-level frontogenetical forcing during the overnight hours, and (ii) arrival of deep tropical moisture from TC Erin.

The increased nocturnal low-level frontogenetical forcing and poleward moisture transport was likely aided by the intensification and nearly perpendicular orientation of the low-level jet relative to the baroclinic zone. Low-level jet intensification likely occurred in response to (i) differential cooling over sloping terrain (e.g., Bonner 1968; Uccellini 1980), and (ii) the increasing geopotential height gradient between TC Erin and the strengthening ridge over the southeast United States. The vertical secondary circulation associated with low-level frontogenetical forcing has been shown to assist in the pooling of elevated moisture along the baroclinic zone to help fuel eastward-propagating MCSs (e.g., Trier et al. 2006). In the case of the TC Erin PRE, however, the vertical secondary circulation lifted parcels to their level of free convection in the nearly moist adiabatic conditions; a direct result of the presence of deep tropical moisture from TC Erin.

As shown by the ECMWF EPS forecasts for the TC Erin case, many of these PREs are associated with synoptic-scale patterns that would have produced rain events whether a TC was present or not (e.g., Maddox et al. 1979; Doswell et al. 1996; Schumacher and Johnson 2005). It is apparent that the role of the TC is to provide deep tropical moisture that can be transported poleward to produce anomalously high moisture values in midlatitudes. This deep tropical moisture from TCs can increase precipitation efficiencies (e.g., Market et al. 2003) and provide a sizeable supply of moisture to sustain deep convection, given adequate synoptic and mesoscale forcing. The nearly moist neutral atmospheric conditions accompanying these TC moisture plumes can allow for PRE formation even in the presence of only weak forcing for

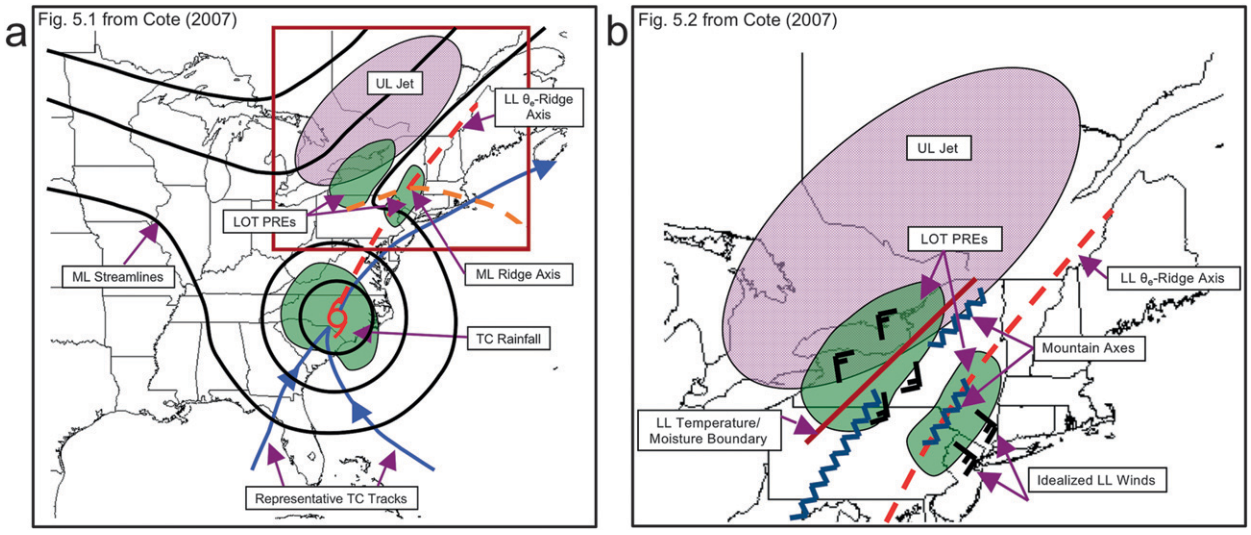

FIG. 24. (a) Conceptual model of the synoptic-scale environment associated with LOT and AC PREs in advance of TCs, revised and updated from Bosart and Carr (1978). Position of TC is given by the tropical storm symbol. Representative TC tracks are marked with solid blue arrows. Low-level (LL) features are representative of the 925-hPa level, midlevel (ML) features are representative of the 700-hPa level, and upper-level (UL) features are representative of the 200-hPa level. (b) Boxed region from (a) indicating the area of the mesoscale and physiographic conceptual model. [Reproduced from Figs. 5.1 and 5.2 in Cote (2007).]

ascent. The presence of TC moisture can turn a heavy rain event into a record-breaking high-impact heavy rain event. Forecasters now have the ability to monitor these deep tropical moisture plumes in real time on an hourly basis by using, for example, the satellite-derived NOAA/NESDIS Blended TPW product. A forthcoming manuscript will use numerical simulations to quantify the effect of TC moisture on accumulated rainfall totals during the TC Erin PRE. Other items for future consideration include 1) assessing the importance of TC-related diabatic outflow in downstream upper-level ridge amplification and jet intensification, as suggested by the PRE-relative composite results, using numerical simulations; and 2) examining and comparing more closely PREs as a function of the size and intensity of their parent TCs.

Acknowledgments. This work was supported by National Science Foundation Grant ATM-0553017 and Collaborative Science, Technology, and Applied Research Program (CSTAR) Grant NA07NWS4680001. The authors thank Prof. Daniel Keyser (University at Albany, SUNY), Matthew Cote (Meso, Inc.), and Michael Jurewicz (NWS Binghamton) for their insights on PREs during the course of this study. Sheldon Kusselson (NOAA/NESDIS) and two anonymous reviewers provided valuable comments and suggestions during the review process. Fruitful discussions with Prof. John Gyakum (McGill University), and Drs. Eyad Atallah (McGill University), Stanley Trier (NCAR), Morris Weisman (NCAR), and Chris Fogarty (Canadian Hurricane Centre) also contributed to this work. The authors thank Dr. Seth Gutman (NOAA/Earth System Research Laboratory) for providing the GPS-Met PW data; Prof. Anantha Aiyyer (North Carolina State University) for providing the air parcel trajectory calculation software; Jason Cordeira (University at Albany, SUNY) for providing the air parcel trajectory plotting routine; and Ben Moore (University at Albany, SUNY) for providing PRE cases for addition to the 1995–2008 event list. Rapid Update Cycle data were obtained from the Atmospheric Radiation Measurement (ARM) Program sponsored by the U.S. Department of Energy, Office of Science, Office of Biological and Environmental Research, Environmental Sciences Division.

REFERENCES

Arndt, D. S., J. B. Basara, R. A. McPherson, B. G. Illston, G. D. McManus, and D. B. Demko, 2009: Observations of the overland reintensification of Tropical Storm Erin (2007). *Bull. Amer. Meteor. Soc.,* **90,** 1079–1093.

Atallah, E. H., and L. F. Bosart, 2003: The extratropical transition and precipitation distribution of Hurricane Floyd (1999). *Mon. Wea. Rev.,* **131,** 1063–1081.

——, ——, and A. R. Aiyyer, 2007: Precipitation distribution associated with landfalling tropical cyclones over the eastern United States. *Mon. Wea. Rev.,* **135,** 2185–2206.

Augustine, J. A., and F. Caracena, 1994: Lower-tropospheric precursors to nocturnal MCS development over the central United States. *Wea. Forecasting,* **9,** 116–135.

Avila, L. A., and E. N. Rappaport, 1996: Atlantic hurricane season of 1994. *Mon. Wea. Rev.,* **124,** 1558–1578.

Beven, J. L., II, S. R. Stewart, M. B. Lawrence, L. A. Avila, J. L. Franklin, and R. J. Pasch, 2003: Annual summary: Atlantic hurricane season of 2001. *Mon. Wea. Rev.,* **131,** 1454–1484.

Bluestein, H. B., 1992: *Principles of Kinematics and Dynamics*. Vol. 1, *Synoptic-Dynamic Meteorology in Midlatitudes,* Oxford University Press, 431 pp.

Bonner, W. D., 1968: Climatology of the low-level jet. *Mon. Wea. Rev.,* **96,** 833–850.

Bosart, L. F., and F. H. Carr, 1978: A case study of excessive rainfall centered around Wellsville, New York, 20–21 June 1972. *Mon. Wea. Rev.,* **106,** 348–362.

——, and D. B. Dean, 1991: The Agnes rainstorm of June 1972: Surface feature evolution culminating in inland storm redevelopment. *Wea. Forecasting,* **6,** 515–537.

——, and G. M. Lackmann, 1995: Postlandfall tropical cyclone reintensification in a weakly baroclinic environment: A case study of Hurricane David (September 1979). *Mon. Wea. Rev.,* **123,** 3268–3291.

Brooks, H. E., and D. J. Stensrud, 2000: Climatology of heavy rain events in the United States from hourly precipitation observations. *Mon. Wea. Rev.,* **128,** 1194–1201.

Buizza, R., C. Cardinali, G. Kelly, and J.-N. Thépaut, 2007: The value of observations. Part II: The value of observations located in singular-vector-based target areas. *Quart. J. Roy. Meteor. Soc.,* **133,** 1833–1842.

Caracena, F., R. A. Maddox, L. R. Hoxit, and C. F. Chappell, 1979: Mesoanalysis of the Big Thompson storm. *Mon. Wea. Rev.,* **107,** 1–17.

Carr, F. H., and L. F. Bosart, 1978: A diagnostic evaluation of rainfall predictability for Tropical Storm Agnes, June 1972. *Mon. Wea. Rev.,* **106,** 363–374.

Chapman, W. T., and Y. T. Sloan, 1955: The paths of Hurricanes Connie and Diane. *Mon. Wea. Rev.,* **83,** 171–180.

Chappell, C. F., 1986: Quasi-stationary convective events. *Mesoscale Meteorology and Forecasting,* P. S. Ray, Ed., Amer. Meteor. Soc., 289–309.

Colle, B. A., 2003: Numerical simulations of the extratropical transition of Floyd (1999): Structural evolution and responsible mechanisms for heavy rainfall over the northeast United States. *Mon. Wea. Rev.,* **131,** 2905–2926.

Corbosiero, K. L., M. J. Dickinson, and L. F. Bosart, 2009: The contribution of eastern North Pacific tropical cyclones to the rainfall climatology of the southwest United States. *Mon. Wea. Rev.,* **137,** 2415–2435.

Cote, M. R., 2007: Predecessor rain events in advance of tropical cyclones. M.S. thesis, Department of Atmospheric and Environmental Sciences, University at Albany, State University of New York, 200 pp. [Available online at http://cstar.cestm.albany.edu/CAP_Projects/Project10/index.htm.]

Davis, R. S., 2001: Flash flood forecast and detection methods. *Severe Convective Storms, Meteor. Monogr.,* No. 50, Amer. Meteor. Soc., 481–525.

Doswell, C. A., III, H. E. Brooks, and R. A. Maddox, 1996: Flash flood forecasting: An ingredients-based methodology. *Wea. Forecasting,* **11,** 560–581.

Dunn, G. E., W. R. Davis, and P. L. Moore, 1955: Hurricanes of 1955. *Mon. Wea. Rev.,* **83,** 315–326.

Franklin, J. L., and D. P. Brown, 2008: Atlantic hurricane season of 2006. *Mon. Wea. Rev.,* **136,** 1174–1200.

Galarneau, T. J., Jr., L. F. Bosart, and R. S. Schumacher, 2009: Reintensification of Tropical Storm Erin (2007) over Oklahoma. *Bull. Amer. Meteor. Soc.,* **90,** 306–308.

Glass, F. H., D. L. Ferry, J. T. Moore, and S. M. Nolan, 1995: Characteristics of heavy convective rainfall events across the mid-Mississippi valley during the warm season: Meteorological conditions and a conceptual model. Preprints, *14th Conf. on Weather Analysis and Forecasting,* Dallas, TX, Amer. Meteor. Soc., 34–41.

Hart, R. E., and R. H. Grumm, 2001: Using normalized climatological anomalies to rank synoptic-scale events objectively. *Mon. Wea. Rev.,* **129,** 2426–2442.

Higgins, R. W., W. Shi, E. Yarosh, and R. Joyce, cited 2000: Improved United States precipitation quality control system and analysis. NCEP/Climate Prediction Center Atlas 7. [Available online at http://www.cpc.ncep.noaa.gov/research_papers/ncep_cpc_atlas/7/toc.html.]

Hoskins, B. J., I. Draghici, and H. C. Davies, 1978: A new look at the omega equation. *Quart. J. Roy. Meteor. Soc.,* **104,** 31–38.

Jarvinen, B. R., C. J. Neumann, and M. A. S. Davis, 1984: A tropical cyclone data tape for the North Atlantic basin, 1886–1983: Contents, limitations, and uses. NOAA Tech. Memo. NWS NHC 22, 24 pp. [Available online at http://www.nhc.noaa.gov/pdf/NWS-NHC-1988-22.pdf.]

Jones, S. C., and Coauthors, 2003: The extratropical transition of tropical cyclones: Forecast challenges, current understanding, and future directions. *Wea. Forecasting,* **18,** 1052–1092.

Junker, N. W., R. S. Schneider, and S. L. Fauver, 1999: A study of heavy rainfall events during the Great Midwest Flood of 1993. *Wea. Forecasting,* **14,** 701–712.

Kalnay, E., and Coauthors, 1996: The NCEP/NCAR 40-Year Reanalysis Project. *Bull. Amer. Meteor. Soc.,* **77,** 437–472.

Keyser, D., M. J. Pecnick, and M. A. Shapiro, 1986: Diagnosis of the role of vertical deformation in a two-dimensional primitive equation model of upper-level frontogenesis. *J. Atmos. Sci.,* **43,** 839–850.

Kistler, R., and Coauthors, 2001: The NCEP–NCAR 50-Year Reanalysis: Monthly means CD-ROM and documentation. *Bull. Amer. Meteor. Soc.,* **82,** 247–267.

Kusselson, S. J., S. Q. Kidder, J. M. Forsythe, and A. S. Jones, 2009: An update on the operational implementation of blended total precipitable water products. Preprints, *23rd Conf. on Hydrology,* Phoenix, AZ, Amer. Meteor. Soc., 8.5. [Available online at http://ams.confex.com/ams/pdfpapers/142967.pdf.]

Luo, M., 2004: Downpour overwhelms transit in morning rush. *New York Times,* 9 September, section 1, A1.

Maddox, R. A., C. F. Chappell, and L. R. Hoxit, 1979: Synoptic and meso-α scale aspects of flash flood events. *Bull. Amer. Meteor. Soc.,* **60,** 115–123.

——, 1980: Mesoscale convective complexes. *Bull. Amer. Meteor. Soc.,* **61,** 1374–1387.

——, L. R. Hoxit, C. F. Chappell, and F. Caracena, 1978: Comparison of meteorological aspects of the Big Thompson and Rapid City flash floods. *Mon. Wea. Rev.,* **106,** 375–389.

Market, P., S. Allen, R. Scofield, R. Kuligowski, and A. Gruber, 2003: Precipitation efficiency of warm-season Midwestern mesoscale convective systems. *Wea. Forecasting,* **18,** 1273–1285.

Moore, J. T., F. H. Glass, C. E. Graves, S. M. Rochette, and M. J. Singer, 2003: The environment of warm-season elevated thunderstorms associated with heavy rainfall over the central United States. *Wea. Forecasting,* **18,** 861–878.

Namias, J., and C. R. Dunn, 1955: The weather and circulation of August 1955. *Mon. Wea. Rev.,* **83,** 163–170.

NCDC, 2007: *Storm Data*. Vol. 49, No. 8, 530 pp.

Pierce, C. H., 1939: The meteorological history of the New England hurricane of Sept. 21, 1938. *Mon. Wea. Rev.,* **67,** 237–285.

Pontrelli, M. D., G. Bryan, and J. M. Fritsch, 1999: The Madison County, Virginia, flash flood of 27 June 1995. *Wea. Forecasting,* **14,** 384–404.

Schumacher, R. S., and R. H. Johnson, 2005: Organization and environmental properties of extreme-rain-producing mesoscale convective systems. *Mon. Wea. Rev.,* **133,** 961–976.

——, and ——, 2006: Characteristics of U.S. extreme rain events during 1999–2003. *Wea. Forecasting,* **21,** 69–85.

——, and ——, 2008: Mesoscale processes contributing to extreme rainfall in a midlatitude warm-season flash flood. *Mon. Wea. Rev.,* **136,** 3964–3986.

——, and ——, 2009: Quasi-stationary, extreme-rain-producing convective systems associated with midlevel cyclonic circulations. *Wea. Forecasting,* **24,** 555–574.

Schwarz, F. K., 1970: The unprecedented rains in Virginia associated with the remnants of Hurricane Camille. *Mon. Wea. Rev.,* **98,** 851–859.

Srock, A. F., and L. F. Bosart, 2009: Heavy precipitation associated with southern Appalachian cold-air damming and Carolina coastal frontogenesis in advance of weak landfalling Tropical Storm Marco (1990). *Mon. Wea. Rev.,* **137,** 2448–2470.

Trier, S. B., C. A. Davis, D. A. Ahijevych, M. L. Weisman, and G. H. Bryan, 2006: Mechanisms supporting long-lived episodes of propagating nocturnal convection within a 7-day WRF model simulation. *J. Atmos. Sci.,* **63,** 2437–2461.

Uccellini, L. W., 1980: On the role of upper tropospheric jet streaks and leeside cyclogenesis in the development of low-level jets in the Great Plains. *Mon. Wea. Rev.,* **108,** 1689–1696.

——, and D. R. Johnson, 1979: The coupling of upper and lower tropospheric jet streaks and implications for the development of severe convective storms. *Mon. Wea. Rev.,* **107,** 682–703.

Wang, Y., Y. Wang, and H. Fudeyasu, 2009: The role of Typhoon Songda (2004) in producing distantly located heavy rainfall in Japan. *Mon. Wea. Rev.,* **137,** 3699–3716.